The role of NPxY domains in LRP1 receptor maturation and function

Dissertation

zur Erlangung des Grades

„Doktor

der Naturwissenschaften"

am Fachbereich Biologie

der Johannes Gutenberg-Universität

in Mainz

von

Thorsten Pflanzner

geboren am 27. Februar 1981

in Nürnberg

Mainz, im Dezember 2010

Dekan:

1. Berichterstatter:

2. Berichterstatter:

Tag der mündlichen Prüfung:

TABLE OF CONTENTS

1. INTRODUCTION

1.1. The low density lipoprotein receptor-related protein 1 (LRP1)

LRP1, also known as α_2-macroglobulin (α_2M) receptor, is a member of the low density lipoprotein-receptor family. It is synthesised as a 600 kDa full-length precursor in the endoplasmatic reticulum (ER) before LRP1 is transfered to the Golgi network. Furin cleavage in the trans-Golgi generates mature LRP1 which is shuttled to the cell surface (Willnow et al., 1996). Cleavage by furin results in an 85 kDa transmembrane β-subunit that remains non-covalently linked to the extracellular 515 kDa α-subunit. The α-subunit consists of 4 clusters of complement-type repeats responsible for ligand binding, whereby clusters II and IV play a dominant role (Neels et al., 1999). To date, more than 40 ligands have been identified, suggesting that LRP1 is involved in a diverse range of (patho)physiologic processes (Herz and Strickland, 2001). The β-subunit has a membrane proximal (1) and a membrane distal (2) asparagin-prolin-x-tyrosine (NPxY) motif, whereby x refers to any amino acid (Figure 1). Whereas the NPxY1 motif seems to play a dominant role in receptor recycling (van Kerkhof et al., 2005), the tyrosine within the NPxY2 domain is necessary for LRP1 endocytosis (Li et al., 2000). Other functions of the NPxY motifs include adaptor protein binding and signal transduction (Herz and Strickland, 2001). LRP1 is predominantly expressed in the brain and liver, but it can be found in almost all other cell types (Moestrup et al., 1992).

1.2. Early embryonic lethality of LRP1 deficient mice

Most of the above mentioned results were obtained *in vitro* in an overexpression system with LRP1 mini-receptors with a largely reduced extracellular domain, since experimental research on LRP1 function *in vivo* by a genetic approach is impaired due to embryonic lethality of the LRP1 knock-out (KO) mouse (Herz et al., 1992). Herz and colleagues found that disruption of the LRP1 gene in mice blocks embryo implantation of LRP1-deficient blastocysts around embryonic day (E) 10. However, when preimplanted blastocysts were isolated at E 3.5, there

5

was no difference between LRP1 KO and wild-type (WT) blastocysts. Both genotypes

appeared normal and could be passaged for up to 20 days.
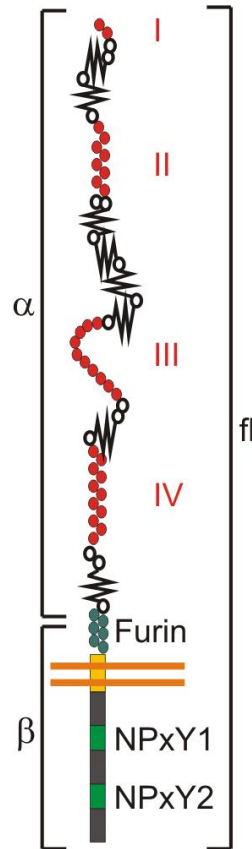
Figure 1 Schematic illustration of LRP1. Immature full-length (fl) LRP1 is cleaved by furin into two non-covalently associated subunits. The 85 kDa transmembrane LRP1-β subunit contains two intracellular NPxY motifs for adaptor protein binding and internalisation. LRP1-α has a molecular weight of 515 kDa and is characterised by four extracellular ligand binding domains (I-IV) for more than 40 ligands.

Determination of the LRP1 WT expression pattern in early postimplantation embryos

revealed a strong LRP1 expression in embryonic tissues, e.g. in primary giant invading

trophoblast cells. Taken together, this suggests that LRP1 plays a role in trophoblast-mediated

invasion of the embryo into the maternal uterine wall. One possible mechanism behind

impaired blastocyst implantation might be LRP1-mediated clearance of plasminogen activator

inhibitor (PAI) complexes in cultured cells (Orth et al., 1992). The urokinase-type

plasminogen activator (uPA) and its receptor uPAR have been shown to be involved in the

control of extracellular matrix (ECM) turnover and tumour invasion by activating the serine

protease plasmin from its precursor plasminogen (Hildenbrand et al.). Therefore, PAI binding to uPA interferes with plasmin activation. Since uPA and LRP1 are both expressed in giant invading trophoblast cells (Sappino et al., 1989), Herz and colleagues investigated whether LRP1 endocytoses pre-complexed uPA-PAI-1. They found that LRP1 binds and internalises the uPA-PAI-1 complex, targeting it for lysosomal degradation (Herz et al., 1992). In their proposed model, LRP1 acts as a scavenger receptor for PAI-inactivated uPA by clearing the complex from the cell surface. In the absence of LRP1, inactive uPA-PAI accumulates on the cell surface and limits plasmin activation, thereby interfering with embryo implantation in the maternal uterine wall.

A second LRP1 mouse model showing early embryonic lethality was recently described (Reekmans et al., 2010; Roebroek et al., 2006). In contrast to the complete LRP1 KO, a recombinase-mediated cassette exchange (RMCE) knock-in procedure was used to modify the endogenous LRP1 gene. Alanine (A) subsititutions within the NPxY domains (NPxY → AAxA) caused distinct phenotypes. Whereas the NPxY2 mutant mouse does not show any obvious phenotype, inactivation of the membrane proximal NPxY1 motif or a combined NPxY1+2 mutation resulted in embryonic lethality. Single NPxY1 knock-in mice died between E 15.5 and E 19 and NPxY1+2 mice around E 10 and E 13.5, highlighting the importance of the membrane proximal NPxY1 motif in LRP1 function (Reekmans et al., 2010; Roebroek et al., 2006).

1.3. LRP1 in Alzheimer's Disease (AD)

AD is the most common age-related neurodegenerative disorder, representing 60-80% of all dementias. Considering increased live expectancy in the 1st world countries and the current rate of AD development, there will be more than 140 million AD cases worldwide by 2050 (Pahnke et al., 2009). Macroscopically, AD pathology is characterised by brain atrophy in the hippocampus and cortex, resulting in cognitive decline and dementia. In histological

specimens, neurofibrillary tangles and amyloid-β (Aβ) plaques, as well as synaptic and neuronal loss, have been extensively described in susceptible brain regions. Neurofibrillary tangles are intraneuronally located ubiquitinated and hyperphosphorylated tau protein bundles, whereas plaques consist of extracellular deposits of hydrophobic Aβ peptides. Aβ is a 36-46 amino acid residue peptide that is proteolytically generated from the type I transmembrane amyloid precursor protein (APP). To circumvent toxic effects mediated by Aβ, several mechanisms of Aβ elimination have been postulated. These can be summarised into three main categories: (i) Enzymatic degradation by proteases, such as insulin-degrading enzyme and neprilysin (Farris et al., 2007; Iwata et al., 2001; Leissring et al., 2003), (ii) continuous and slow perivascular drainage of Aβ, in conjunction with other solutes and interstitial fluid (ISF) along the walls of arteries and capillaries (Preston et al., 2003; Utter et al., 2008), and (iii) rapid transporter- or receptor-mediated uptake or bidirectional exchanges of soluble Aβ across the blood-brain barrier (BBB) (Tanzi et al., 2004; Wang and Tall, 2003). LRP1 has been linked to AD by its capability to modulate APP processing (Pietrzik et al., 2002). Direct interaction of LRP1 with APP is established by FE65 adaptor protein binding to the NPxY2 domain of LRP1 (Pietrzik et al., 2004). Moreover, LRP1 has recently been shown to be a competitive substrate for APP processing by BACE1 (von Einem et al.). Interestingly, LRP1 can modulate Aβ deposition and AD susceptibility by clearing soluble Aβ from the extracellular space (Kang et al., 2000). Further investigations revealed that LRP1 mediates Aβ transcytosis across the BBB from the brain into the blood (Shibata et al., 2000). To date, genetic evidence for LRP1-mediated transcytosis of Aβ across the BBB is missing due to the embryonic lethal phenotype of LRP1 KO mice.

1.4. The BBB in AD

The BBB separates the circulating blood from the central nervous system (CNS). It is a diffusion barrier essential for maintaining tissue homeostasis of the CNS and prevents the

entry of pathogens (Abbott et al., 2006). Endothelial cells (ECs), astrocytes and pericytes are the cellular components of the BBB (Figure 2). In contrast to ECs from other vascular beds, brain ECs do not show fenestrations and have more extensive tight junctions (TJs) (Madara, 1988). TJs limit the paracellular flux of hydrophilic molecules across the BBB, while small lipophilic substances like O_2 and CO_2 diffuse freely across plasma membranes along their concentration gradient (Grieb et al., 1985). The BBB is further essential for the supply of nutrients to the CNS. Brain ECs express a large number of specialised transporters, including carriers for glucose and amino acids. Other essential factors such as insulin, iron and leptin are transported via receptor-mediated transcytosis (Pardridge et al., 1985; Zhang and Pardridge, 2001). Besides carrier systems that are essential for the supply of nutrients, brain ECs express receptors (e.g. LRP1) that are involved in the pathogenesis of AD (Pflanzner et al., in press).
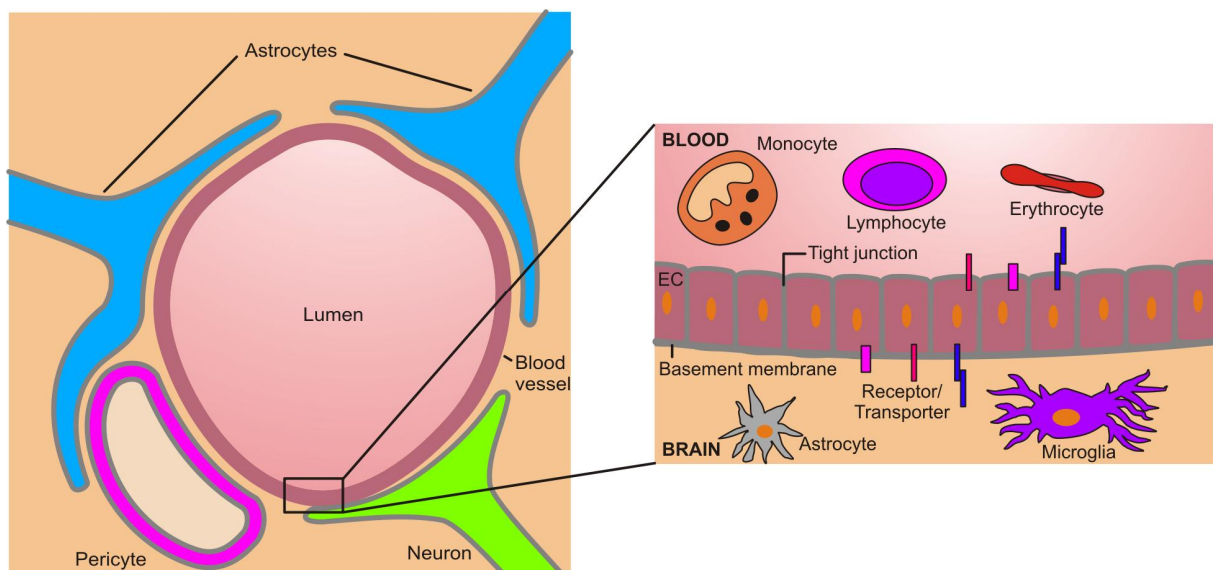
Figure 2   The neurovascular unit establishes the blood-brain barrier (BBB) *in vivo*. Blood vessels are in contact with astrocytic endfeet, neurons and pericytes (left panel). Endothelial cells (ECs) form a polarised monolayer through interaction with the abluminal basement membrane (right panel). Expression of luminal and abluminal residing receptors and transporters facilitates exchange of compounds between blood stream and brain. This is necessary due to the insulator function of the BBB. Free exchange of solutes and toxins between blood and brain is restricted by the expression of tight junctions at EC borders.

Although the function of the BBB during AD is poorly understood some alterations in the structure and the integrity have been observed (Bowman et al., 2007). In AD post-mortem

brains an upregulation of $\alpha_v\beta_3$-integrin can be detected, a marker of angiogenesis and vascular densities. The latter positively correlates with Aβ load in the hippocampus of AD patients (Desai et al., 2009). Angiogenic vessels differ from already existing vessels in that they have widened interendothelial junctions, numerous fenestra, abnormal cell shape and basement membrane (Carmeliet and Jain, 2000). Considering the increased leakiness of newborn vessels in AD, an abnormal exchange of solutes can occur, therefore, interfering with physiologic processes. Numerous studies on the effect of Aβ on endothelium have been conducted. It has been demonstrated that Aβ peptides are toxic to neuromicrovascular ECs *in vitro*, induce apoptosis, stimulate superoxide radical production and the expression of inflammatory genes, resulting in an alteration of the structure and function of ECs (Blanc et al., 1997; Folin et al., 2005; Thomas et al., 1996; Vukic et al., 2009). Furthermore, Aβ aggregates, not monomers or fibrils, can induce a redistribution of TJ molecules from the plasma membrane into the cytosol resulting in decreased barrier tightness (Gonzalez-Velasquez et al., 2008). A recent study showed a decrease in capillary number and diameter, thereby offering less surface for Aβ clearance across the BBB (Bouras et al., 2006). Further analysis revealed a downregulation of homeobox gene Meox2, a regulator of vascular differentiation, as the key player involved in reduced brain capillary density in AD (Wu et al., 2005). Overall, it can be hypothesised that altered capillary morphology and physiology, as well as inflammatory responses, are of major importance for AD pathogenesis. Here, we focus on Aβ clearance mechanisms across the BBB (Figure 3).

1.4.1. Transporter-mediated clearance

Transporter-mediated clearance of Aβ at the BBB is facilitated by ATP-binding cassette (ABC) transporter family members. They can be found in all organisms and resemble the largest family of active transport molecules (Higgins, 1992). Eukaryotic ABC transporters mediate efflux of cytoplasmic or plasma membrane associated molecules into the extracellular

space. They consist of two hydrophobic membrane spanning segments with a pair of ATP-binding domains, whereas ATP hydrolysis is generally believed to drive active efflux of ABC transporter substrates (Dean et al., 2001). Their main physiologic function is to restrict tissue penetration by mediating reverse efflux of a substrate through its pore, e.g. a compound enters an EC at the BBB and is then effluxed back into the blood stream.

Three ABC transporters have been implicated to play a role in Aβ clearance across the BBB. ABCA1 has been described to facilitate the transfer of cellular cholesterol from the endothelium into the blood, hence, resembling the rate-limiting step in atherosclerosis prevention (Van Eck et al., 2005). Wahrle and colleagues crossed ABCA1$^{-/-}$ mice into a mutant human APP overexpressing AD mouse model and analysed APP processing and brain Aβ levels. Whereas APP processing was not altered, they found an increase in soluble Aβ40 in the brain and the development of cerebral amyloid angiopathy (CAA) was more common compared to controls, indicating towards a role for ABCA1 in clearing Aβ across the BBB (Wahrle et al., 2005). A stereotactic brain microinjection experiment however failed to show ABCA1-mediated Aβ transport from brain-to-blood. The amount of radiolabelled Aβ injected into the brain was not significantly different between ABCA1$^{-/-}$ and control animals (Akanuma et al., 2008). Thus, further studies need to be conducted to clear the relevance of ABCA1 in this paradigm.

BCRP, also called ABCG2, was identified as multi-drug resistance efflux transporter in MCF-7 breast cancer cells (Doyle et al., 1998). Xiong and colleagues found that Aβ co-immunoprecipitates with BCRP and, further, interferes with BCRP-mediated drug efflux (Xiong et al., 2009). In addition, Aβ tail vein injection experiments revealed that Aβ enters the brain to a higher degree in BCRP$^{-/-}$ animals compared to controls. This result was underlined in an *in vitro* model of the BBB. Addition of a BCRP inhibitor increased the Aβ clearance quotient in the blood-to-brain direction, whereas no effect was observed in the

brain-to-blood direction (Tai et al., 2009). This suggests that BCRP acts as a gatekeeper for Aβ at the BBB, limiting Aβ entry from the blood into the brain.

P-glycoprotein (P-gp) is the best described ABC transporter family member involved in Aβ clearance at the BBB. Both *in vivo* and *in vitro* studies have shown that P-gp can clear Aβ in the brain-to-blood direction (Cirrito et al., 2005; Kuhnke et al., 2007). In addition, a role for P-gp in the prevention of Aβ entry into the brain has been described (Tai et al., 2009). There have also been studies that failed to show a role for P-gp-mediated Aβ clearance. Pre-administration of P-gp inhibitors into the brain did not alter Aβ clearance across the BBB (Ito et al., 2006). It has to be noted that P-gp is expressed at the luminal EC membrane and application of a P-gp inhibitor into the periphery succeeded in reducing Aβ clearance from brain-to-blood (Cirrito et al., 2005).
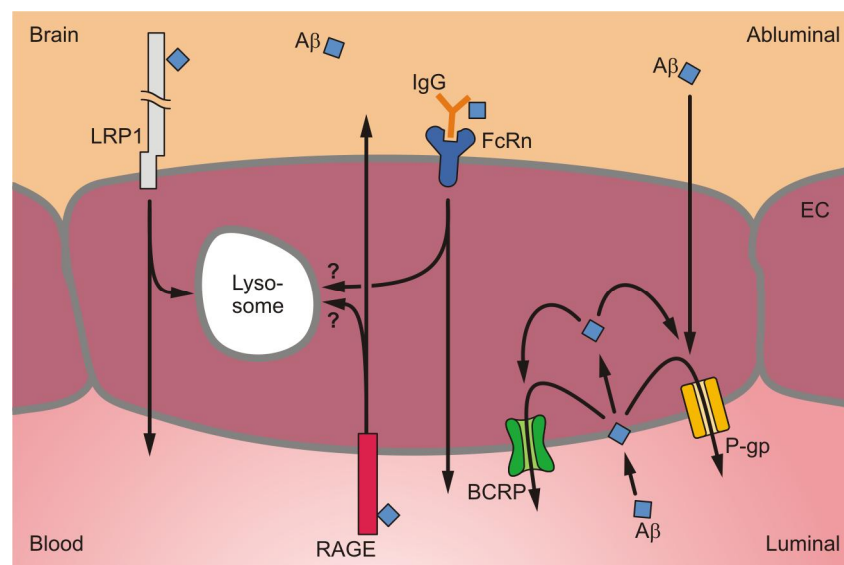
Figure 3   Clearance of amyloid-β (Aβ) at the blood-brain barrier (BBB). Low density lipoprotein receptor-related protein 1 (LRP1) is predominantly expressed at the abluminal membrane of brain capillaries and mediates Aβ clearance from the brain, via transcytosis into the blood, and Aβ degradation in the endosomal/lysosomal pathway. Neonatal Fc receptor (FcRn) mediates IgG-assisted clearance of brain parenchymal Aβ into the blood via transcytosis. Luminally expressed receptor for advanced glycation endproducts (RAGE) transcytoses circulating Aβ from the periphery into the brain. Both FcRn and RAGE might also be involved in Aβ clearance via the endosomal/lysosomal pathway. ABC transporter-mediated clearance of Aβ from the brain is facilitated by P-glycoprotein (P-gp). Both, breast cancer resistance protein (BCRP) and P-gp are expressed on the luminal membrane of endothelial cells (ECs), hence, they can act as Aβ gatekeeper at the BBB to prevent its entry into the brain. Due to the controversial role of ABCA1 in Aβ clearance at the BBB it is not displayed.

1.4.2. Receptor-mediated clearance

Upon ligand binding to a transmembrane receptor the complex is internalised and can enter various pathways, e.g. endosomal/lysosomal pathway, recycling or transcytosis. Receptor-mediated clearance across an endothelial barrier involves transcytosis. Transcytosis is characterised by internalisation into endosomal vesicles, followed by transit through the cell upon which the vesicle fuses with the opposite plasma membrane and the receptor releases its ligand due to pH changes.

To date, Aβ clearance across the BBB has been described for three transmembrane receptors. Among them is the major histocompatibility complex class I-related neonatal Fc receptor (FcRn). FcRn has been well described for the transfer of passive immunity from mother to fetus across the placenta (Simister and Mostov, 1989). Residing on the abluminal membrane in brain ECs, FcRn has also been described in mediating IgG-assisted Aβ clearance from the brain into the blood (Deane et al., 2005; Schlachetzki et al., 2002). Aβ-specific IgG 4G8 formed a stable complex with Aβ and is cleared faster in the brain-to-blood direction than Aβ alone. The 4G8-Aβ complex transported into the blood was 100% trichloroacetic acid precipitable pointing towards a transcytotic mechanism.

Under physiologic conditions high expression levels of the pattern recognition receptor for advanced glycation end products (RAGE) are only found in the lung, but low levels can be found in many differentiated adult cells such as the endothelium (Schmidt et al., 1994; Xie et al., 2008). In contrast to FcRn, RAGE mediates Aβ influx from the periphery into the brain. Mackic and colleagues found that surface binding of Aβ to the luminal membrane of primary human brain microvascular ECs was time-dependent and inhibitable by RAGE antibody. Further, in an *in vitro* model of the BBB, blood-to-brain transcytosis of Aβ was time- and temperature-dependent, and also could be blocked by RAGE-specific antibody (Mackic et al., 1998). These findings were confirmed by *in vivo* studies investigating RAGE-mediated Aβ transport from blood-to-brain. Systemically infused Aβ was RAGE-dependently endocytosed

by brain capillaries and transported across the BBB, whereas RAGE$^{-/-}$ mice showed no Aβ transport into the brain (Deane et al., 2003). In addition, LaRue and colleagues found an 8 fold increase in Aβ transport from blood-to-brain in 5 to 6 month-old Tg2576 mice due to RAGE upregulation (LaRue et al., 2004).

Most data for receptor-mediated Aβ clearance across the BBB has been collected for LRP1. Shibata and colleagues reported a rapid vascular clearance of Aβ from brain-to-blood across the BBB that can be inhibited by the receptor-associated protein (a ligand binding inhibitor for LRP1), an N-terminal LRP1 antibody and α$_2$M (Shibata et al., 2000). In addition, AD patient samples showed reduced LRP1 staining in the brain vasculature compared to non-AD controls, correlating with regional Aβ accumulation. Aβ42 and mutant, vasculotropic Dutch/Iowa (DI) Aβ40 show a reduced binding affinity to immobilised LRP1, when compared to Aβ40, resulting in a decreased LRP1-mediated uptake into brain capillaries (Deane et al., 2004). This could result in decreased clearance of vasculotropic DI Aβ40 by brain capillaries and has been postulated to participate in CAA development. Furthermore, soluble circulating LRP1 (sLRP1) has been shown to be the major binding protein of Aβ in plasma mediating peripheral 'sink' activity on Aβ in the brain and, targeting the sLRP1-Aβ complex for degradation by the liver, kidney and spleen (Sagare et al., 2007). Although several studies show a role for LRP1 in Aβ clearance from brain-to-blood, recently, Nazer and colleagues suggested that LRP1 rather mediates endocytosis and degradation of Aβ than transcytosis by using a kidney epithelial cell line overexpressing LRP1 (Nazer et al., 2008).

1.5. Aims of the study

We set out to investigate the early embryonic to perinatal lethal phenotype of NPxY1 and NPxY1+2 mutant LRP1 knock-in mice (Reekmans et al., 2010; Roebroek et al., 2006). Hence, mouse embryonic fibroblasts (MEFs) generated from each of the NPxY mutant mice

(NPxY1/NPxY2/NPxY1+2) were analysed for LRP1 production, maturation, endocytosis and degradation.

To date, LRP1-mediated transcytosis across the BBB is controversial due to lack of genetic evidence and a recent study that failed to show a role for LRP1-mediated transcytosis but rather demonstrated a role for LRP1 in Aβ endocytosis and degradation (Herz et al., 1992; Nazer et al., 2008; Shibata et al., 2000). We analysed the possible involvement of LRP1 in mediating Aβ transcytosis across primary mouse brain capillary ECs (pMBCECs). Based on the results of LRP1 NPxY knock-in mice, this *in vitro* BBB model could provide genetic evidence for the participation of LRP1 in Aβ transport across BBB. Furthermore, we investigated if LRP1 acts as a receptor for bidirectional transcytosis of Aβ across the BBB.

2. MATERIALS AND METHODS

2.1. Sodium dodecylsulfate-polyacrylamide gel electrophoresis (SDS-PAGE) and Western blot analysis of cell surface biotinylation experiments

Mouse embryonic fibroblast (MEF) cells were generated from low density lipoprotein receptor-related protein 1 (LRP1) knock-in mice, in which the intracellular NPxY domains were replaced by alanines (Reekmans et al., 2010; Roebroek et al., 2006). LRP1 wild-type (WT) and knock-in MEFs carrying a single inactivation of the NPxY1 or NPxY2 motif, as well as a cell line with combined inactivation (NPxY1+2) were grown in Dulbecco's modified Eagle medium (DMEM)-F12 (Lonza, Cologne, Germany) supplemented with 10% fetal calf serum (FCS; Invitrogen, Darmstadt, Germany), 100 U/mL penicillin and 100 µg/mL streptomycin (Gibco, Darmstadt, Germany), at 37 °C and 5% CO_2 to near confluence in 6 cm dishes. Prior to biotinylation, cells were washed twice with ice-cold PBS (Gibco) and incubated for 40 minutes with 0.5 mg/ml membrane impermeable EZ-link Sulfo NHS-LC-LC-Biotin (Pierce, Bonn, Germany) in ice-cold PBS. Dishes were washed 4 times with ice-cold PBS containing 50 mM NH_4Cl to quench any unconjugated biotin. Cells were then lysed in 600 µl NP40 lysis buffer (50 mM Tris-HCl, 150 mM NaCl, 0.02% NaN_3, 1% Nonidet P40) containing protease inhibitors (Roche, Mannheim, Germany) and protein content was determined by bicinchoninic (BCA) Protein Assay (Pierce). Four hundred µg of protein was precipitated with NeutrAvidin beads (dilution 1:20; Pierce) overnight at 4°C. Beads were washed twice in NP40 lysis buffer and subsequently incubated in SDS sample buffer containing β-mercaptoethanol (Roth, Karlsruhe, Germany). Twenty µg of whole cell lysates incubated in SDS buffer were used as input control. Samples were boiled in SDS for 5 minutes at 95 °C followed by protein separation on 4-12% bis-tris gels (Invitrogen) and transfer to nitrocellulose membranes (Whatman, Karlsruhe, Germany) for 2 hours at 70 V and at 4 °C. Membranes were blocked in tris-buffered saline containing 0.1% Tween 20 (Roth) and 5% milk. For detections, rabbit polyclonal anti-1704 (dilution 1:10000) recognising the

C-terminus of LRP1 and mouse monoclonal anti-tubulin (dilution 1:2500; Sigma, Schnelldorf, Germany) antibodies were used (Pietrzik et al., 2002). Secondary antibodies linked to horseradish peroxidase (dilution 1:10000; Jackson Laboratory, Sulzfeld, Germany) were used and protein bands were visualised by ECL reagent (Millipore, Schwalbach, Germany).

2.2. Analysis of LRP1 biosynthesis in pulse-chase experiments

Confluent cultures of MEFs were starved for 1 hour in DMEM deprived of methionine/cysteine (Met/Cys; Gibco) and subsequently pulse labelled for 1 hour with Met/Cys-free DMEM, supplemented with 150 µCi/ml [^{35}S]-Met/Cys (Perkin Elmer, Boston, MA, USA) and 20 mM 4-(2-hydroxyethyl)-1-piperazineethanesulfonic acid (HEPES; Lonza) at 37 °C. Cells were immediately lysed in NP40 as described above or chased for 6, 12, 24 or 48 hours in DMEM-F12 growth medium supplemented with 20 mM HEPES. LRP1 was immunoprecipitated overnight at 4 °C with 1704 antibody (dilution 1:300) in the presence of Protein A Agarose beads (dilution 1:20; Invitrogen) in NP40. Immunoprecipitates were washed three times with NP40 lysis buffer and boiled in LDS sample buffer. Proteins were separated on 4-12% bis-tris gels (Invitrogen) under denaturing, reducing conditions and dried on Whatman paper (Whatman). Quantification was performed with a phospor-imager (BAS 1800; Fujifilm, Düsseldorf, Germany) and AIDA software (Raytest, Straubenhardt, Germany). Results represent the mean + SEM of 3 independent experiments.

2.3. Brefeldin A (BFA) and monensin treatment

Subconfluent MEF cell lines were incubated with 10 µg/ml BFA or 5 µM monensin (both from Sigma) in normal growth medium for 5 hours prior to preparation of whole cell lysates in NP40. Dimethyl sulfoxide (DMSO; Roth) was used as solvent control. Cell lysates (20 µg) were boiled in SDS buffer for 5 minutes at 95 °C, before samples were analysed by SDS-

PAGE and Western blotting using 1704 and tubulin antibodies as described in the cell surface biotinylation experiment.

2.4. Proteasomal degradation

Cells were radiolabelled as described in the pulse-chase section in the presence or absence of 50 µM MG132 (Sigma), a proteasome inhibitor. After 1 hour pulse labelling, cells were chased for 4 hours in chase medium containing 50 µM MG132 or DMSO (solvent for MG132) before LRP1 was immunoprecipitated with 1704 antibody. Immunoprecipitation, sample preparation, PAGE and quantification were performed as described in pulse-chase experiment section. Results are expressed as mean + SEM of 3 independent experiments.

2.5. Isolation and cultivation of primary mouse brain capillary endothelial cells (pMBCECs)

pMBCECs were isolated from 6-10 weeks old C57Bl6 WT and C57Bl6/129 LRP1 NPxY2 knock-in mice as previously described (Roebroek et al., 2006; Weidenfeller et al., 2005). In brief, mice were sacrificed by cervical dislocation, the forebrains were pooled, meninges were removed and the tissue was mechanically dissociated, followed by a digest with a mixture of 0.75 mg/ml collagenase CLS2 (Worthington, Lakewood, NJ, USA) and 10 U/ml DNAse (Sigma) in DMEM (Gibco) carried out at 37 °C on a shaker set at 200 rounds per minute for 1 hour. The pellet was resuspended in 20% bovine serum albumin (BSA)-DMEM (w/v) and centrifuged at 1000g for 20 minutes to remove myelin. The pellet was further digested with 1 mg/ml collagenase-dispase (Roche) and 10 U/ml DNAse in DMEM at 37 °C on a shaker for 1 hour. Endothelial capillaries were separated on a 33% continuous Percoll (GE Healthcare, Munich, Germany) gradient, collected and, plated in dishes coated with 0.4 mg/ml collagen IV and 0.1 mg/ml fibronectin (both from Sigma). Cultures were maintained in DMEM supplemented with 20% plasma-derived bovine serum (PDS; First Link, Birmingham, UK),

100 U/ml penicillin and 100 µg/ml streptomycin, 2 mM L-glutamine (Gibco), 4 µg/ml puromycin (Alexis, Loerrach, Germany) and 1 ng/ml basic fibroblast growth factor (R&D Sytems, Wiesbaden, Germany), at 37 °C and 5% CO_2 (Perriere et al., 2005). After three days in culture puromycin was withdrawn and, after reaching confluence on day 5, the culture medium was removed and serum-free DMEM/Ham's F12 (Gibco) medium containing 1 mM L-glutamine, 100 U/ml penicillin, 100 µg/ml streptomycin and 550 nM hydrocortisone (HC; Sigma) was added.

2.6. Transendothelial electrical resistance (TEER) measurements

For measurement of TEER, pMBCECs were grown on 6-well transwell cell culture inserts (Greiner Bio-One, Frickenhausen, Germany) with a membrane pore size of 0.4 µm and 452.4 mm^2 growth surface. TEER was measured with a chopstick electrode connected to an epithelial ohmmeter (both from World Precision Instruments, Berlin, Germany). Background resistance of coated inserts without cells was subtracted from the total resistance of each culture insert containing confluent pMBCECs. TEER was determined in fresh serum free medium on day 5 in culture and 24 hours after incubation with HC containing serum free DMEM/Ham's F12. In all further experiments, pMBCECs were used after 24 hour incubation in HC containing medium. Results are presented as mean + SEM of 25 independent experiments.

2.7. Immunofluorescence confocal microscopy

pMBCECs were washed with PBS and then fixed for 5 minutes at room temperature (RT) with 4% paraformaldehyde (Sigma) in PBS (w/v). Cells were washed with PBS and cell membranes were permeabilised using 0.1% Triton X-100 (Roth) in PBS (PTx; v/v). Non-specific binding was blocked with 4% BSA (Sigma) in PTx (w/v) for 1 hour at RT. Cells were then incubated over night at 4 °C with the following primary antibodies (Santa Cruz

Biotechnology, Heidelberg, Germany) diluted in blocking buffer: rabbit polyclonal anti-ZO-1 (4 µg/ml) and rabbit polyclonal anti-occludin (4 µg/ml). Subsequently, cells were incubated for 4 hours at RT with goat anti-rabbit Alexa 546 secondary antibody (4 µg/ml; Molecular Probes, Darmstadt, Germany) in blocking buffer. After the incubations, samples were washed three times with PTx. Results were visualised using a confocal fluorescence microscope equipped with ZEN 2008 software (LSM710; Carl Zeiss, Jena, Germany).

2.8. Western blot analysis of LRP1 and receptor for advanced glycation end products (RAGE) expression in pMBCECs

Expression of mature LRP1-β subunit and RAGE was analysed in freshly isolated pMBCECs, MEFs, LRP1-deficient CHOs (13-5-1) and rat lung tissue lysed in NP40 buffer containing proteinase inhibitors. For rat lung, CHOs and MEFs, 20 µg protein, and for pMBCECs, 200 µg protein representing all capillaries derived from 10 mice, were analysed. Proteins were separated on a 10% tris-glycine gel and transferred to a nitrocellulose membrane (Whatman). All further steps are described in the Western blotting section of cell surface biotinylation experiments. RAGE expression was analysed with goat anti-RAGE specific IgG (R&D Systems, Wiesbaden, Germany).

2.9. α₂-Macroglobulin (α₂M) endocytosis assay

Internalisation of iodinated α_2M was performed as previously described with minor modifications (Dickson et al., 1981). Shortly, 1 mg α_2M (Calbiochem, Darmstadt, Germany) was dissolved in PBS and subsequently activated with methylamine (Sigma), final concentration 100 nM, for 30 minutes at RT. Activated α_2M/methylamine was dialysed against PBS at 4 °C over night to diminish excess methylamine. PBS was changed every 8 hours. Activated α_2M was iodinated with 1 mCi Na[^{125}I] (Perkin Elmer) by the Chizzonite Indirect Method for Iodination using pre-coated iodination tubes (Pierce). The reaction

mixture was chromatographed on a NAP-5 column (GE Healthcare) to exclude free $Na[^{125}I]$ from iodinated α_2M. BSA was added to a final concentration of 2 mg/ml. Confluent cells were blocked for 30 minutes with medium containing 4 µg/ml BSA and incubated for 1 hour at 37 °C in the respective medium (supplemented with 1 mM Ca^{2+}, 20 mM HEPES, 4 µg/ml BSA) plus 100 µg/ml activated $[^{125}I]$-α_2M. To inhibit α_2M uptake, receptor-associated protein (RAP) was expressed in bacteria as a fusion protein with glutathione S-transferase (GST) and was purified as previously described (Martin et al., 2008). Therefore, RAP-GST or GST was initially added at a final concentration of 500 nM. Subsequently, cells were washed five times with ice-cold PBS. Remaining surface bound $[^{125}I]$-α_2M was removed by two acidic washes with PBS (pH 2) before cells were lysed in 0.2 N NaOH and collected for analysis. Acid-labile and acid-resistant radioactivity represent the surface and internalised pools, respectively. Hence, the ratio of acid-resistant to acid-labile counts provide a measure of the internalised versus cell surface pools of $[^{125}I]$-α_2M. Samples were counted on a Wallac Wizard^2 2470 automatic γ-counter (Perkin Elmer). Results are expressed as mean + SEM of at least two independent experiments.

2.10. $[^{125}I]$-Amyloid-β 1-40 (Aβ$_{1-40}$) kinetics

To analyse the integrity of $[^{125}I]$-Aβ$_{1-40}$ (Perkin Elmer) over a 6 hour time period, 0.1 nM $[^{125}I]$-Aβ$_{1-40}$ was incubated in serum free medium + HC + 40 mM HEPES at 37 °C before samples were subjected to trichloroacetic acid (TCA) precipitation. Fifty µl 15% TCA was added to a 50 µl media sample and incubated for 10 minutes at 4 °C. Samples were then centrifuged at $10000g$ for 10 minutes. Supernatant (free $[^{125}I]$) and pellet (intact $[^{125}I]$-Aβ$_{1-40}$) were counted separately for $[^{125}I]$ on a Wallac Wizard^2 2470 automatic γ-counter (Perkin Elmer). Results are expressed as mean + SEM of three independent experiments. In addition, a 15 µl media sample was collected at each time point to investigate $[^{125}I]$-Aβ$_{1-40}$ oligomerisation. Media samples were mixed with 5 µl SDS sample buffer containing β-

mercaptoethanol and separated on a 16% bis-tris gel. The gel was dried onto Whatman paper and the result was visualised by autoradiography.

2.11. *In vitro* transwell pMBCEC model for transport studies

Our transwell transport model set up resembles a previously published method with minor modifications (Nazer et al., 2008). In brief, freshly isolated pMBCEC fragments were seeded onto coated transwell filters (Greiner Bio-One) with membrane pore size 0.4µm and cultured as described above (Figure 4). After incubation for 24 hours in serum free medium + HC cells were used for transport studies. $[^{125}I]$-A$\beta_{1\text{-}40}$ (0.1 nM; Perkin Elmer) and 1 µCi/ml $[^{14}C]$-inulin (Perkin Elmer) as a marker for paracellular diffusion were added to serum free media + HC + 40 mM HEPES containing 500 nM RAP-GST for LRP1 inhibition or 500 nM GST for control condition and incubated at 37 °C. From each input and at each timepoint, 10 µl and 50 µl samples were taken from the compartment the transport was investigated to (acceptor). Probes were counted on a Wallac Wizard^2 2470 automatic γ-counter (Perkin Elmer) for $[^{125}I]$, or on a Tri-Carb 2800 TR Liquid Scintillation Analyser (Perkin Elmer) for $[^{14}C]$. To investigate the amount of intact $[^{125}I]$-A$\beta_{1\text{-}40}$ being transported, 50 µl 15% TCA was added to a 50 µl media sample and incubated for 10 minutes at 4 °C. Samples were then centrifuged at 10000g for 10 minutes. Supernatant (free $[^{125}I]$) and pellet (intact $[^{125}I]$-A$\beta_{1\text{-}40}$) were counted separately for $[^{125}I]$. Transport of intact $[^{125}I]$-A$\beta_{1\text{-}40}$ across the monolayer was calculated as A$\beta_{1\text{-}40}$ transcytosis quotient (TQ):

$$\text{A}\beta_{1\text{-}40}\,\text{TQ} = \frac{([^{125}I]-A\beta_{1-40})_{acceptor}\big/([^{125}I]-A\beta_{1-40})_{input}}{([^{14}C]-inulin)_{acceptor}\big/([^{14}C]-inulin)_{input}}\ .$$

For 6 hour time course transport studies, pMBCECs were cultured on 6-well transwell inserts (growth surface area 452.4mm^2) with 600 µl media in the upper (luminal) compartment and 1.8 ml in the lower (abluminal) compartment, resembling blood vessel and brain, respectively. $[^{125}I]$-A$\beta_{1\text{-}40}$ and $[^{14}C]$-inulin were added together with RAP-GST or GST to the abluminal

compartment and samples were taken at each time point from the luminal (acceptor) compartment. Results represent mean ± SEM of three independent experiments.
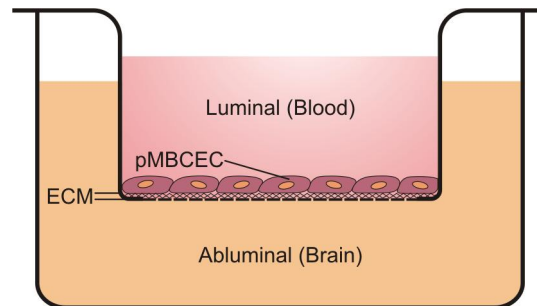

Figure 4   Schematic representation of our *in vitro* blood-brain barrier model. Primary mouse brain capillary endothelial cells (pMBCECs) are cultured on the upper side of transwell inserts coated with extracellular matrix (ECM). ECM, consisting of a mixture of collagen IV/fibronectin, facilitates the polarisation of pMBCEC monolayers, whereby the upper compartment resembles the luminal (blood) side and the lower compartment the abluminal (brain) side.

Surface binding of $[^{125}I]$-Aβ_{1-40} was investigated in 24-well transwell studies (growth surface area 31.2mm^2) with 100 µl media in the luminal and 600 µl in the abluminal compartment. $[^{125}I]$-Aβ_{1-40} and $[^{14}C]$-inulin were added together with RAP-GST or GST to the abluminal compartment and incubated for 15 minutes. Subsequently, both compartments were washed five times with ice-cold PBS and the remaining surface bound $[^{125}I]$-Aβ_{1-40} was removed by acidic washes with PBS (pH 2) from both the abluminal and luminal membrane. $[^{125}I]$-Aβ_{1-40} bound to the abluminal membrane was normalised to total $[^{125}I]$-Aβ_{1-40} of input. $[^{125}I]$-Aβ_{1-40} transcytosed to the luminal membrane was normalised to total $[^{125}I]$-Aβ_{1-40} of input and corrected for inulin permeability (see denominator of TQ). Results represent mean + SEM of three independent experiments in triplicate.

Study of transport from the luminal to abluminal (blood-to-brain) compartment was also performed in 24-well transwell dishes. Monolayers were incubated for 6 hours with $[^{125}I]$-Aβ_{1-40} and $[^{14}C]$-inulin together with RAP-GST or GST in the luminal compartment before samples were taken abluminal. In addition, pMBCEC monolayers derived from LRP1 NPxY2

knock-in mice and WT control littermates were analysed for $A\beta_{1-40}$ transport over a 6 hour time period. Data represent mean + SEM of three independent experiments in triplicate.

Investigation of $[^{125}I]$-$A\beta_{1-40}$ transcytosis across pMBCEC monolayers derived from LRP1 NPxY2 knock-in mice and WT control littermates was conducted in 24-well transwell dishes in the abluminal to luminal (brain-to-blood) direction for 2 hours. $[^{125}I]$-$A\beta_{1-40}$ and $[^{14}C]$-inulin were added to the abluminal compartment and samples were taken from the luminal compartment. Data are expressed as mean + SEM of three independent experiments performed in quadruplicate.

2.12. Statistics

All graphs and statistical analyses were prepared using GraphPad Prism 4 software (GraphPad, La Jolla, CA, USA). Data were analysed by one-way analysis of variance (ANOVA) coupled to Newman-Keuls post test for multiple comparison or t-test. $p < 0.05$ was considered as statistically significant.

3. RESULTS

3.1. Low density lipoprotein receptor-related protein 1 (LRP1) full-length (fl) is present but mature LRP1-β is severely reduced in NPxY1 and NPxY1+2 mutants

Since the complete LRP1 knock-out (KO) is embryonic lethal, LRP1 knock-in mice were generated to study LRP1 function *in vivo* in more detail (Herz et al., 1992; Reekmans et al., 2010; Roebroek et al., 2006). Facilitated by a recombinase-mediated cassette exchange knock-in procedure, the endogenous LRP1 gene was modified within the gene sequence encoding the NPxY motifs. Gene sequence modification resulted in a substitution of the NPxY domains by alanines (NPxY → AAxA). In contrast to the viable NPxY2 knock-in mouse line, the perinatal lethal phenotype of NPxY1 and NPxY1+2 LRP1 knock-in mice points towards a severe impairment of LRP1 function by these NPxY motif mutations. To unravel the mechanism behind the impact of NPxY mutations on the function of LRP1, we studied the steady state expression levels of all LRP1 knock-in mutants compared to wild-type (WT) control in mouse embryonic fibroblast (MEF) cell lines derived from each mutant mouse line. Immature LRP1 is synthesised in the endoplasmatic reticulum (ER) as a 600 kDa fl precursor before it is cleaved by furin in the trans-Golgi. Furin cleavage generates two non-covalently linked subunits representing mature LRP1, an extracellular 515 kDa α–subunit and the 85 kDa transmembrane β–subunit with two cytoplasmatic NPxY motifs. Analysis of whole cell lysates for LRP1 expression levels in all mutants revealed a reduced presence of mature LRP1 in NPxY1 and NPxY1+2 mutant MEFs. Immature LRP1-fl is expressed in all mutant MEFs, whereas the presence of mature LRP1-β is hardly detectable in both MEF cell lines with the NPxY1 motif substitution (Figure 5, left panel). This severe reduction of mature LRP1 upon NPxY1 substitution could explain the perinatal lethal phenotype observed in NPxY1 and NPxY1+2 mutant mice, mimicking the complete LRP1 KO described by Herz and colleagues. In contrast, LRP1-β expression levels in NPxY2 MEFs are comparable to WT MEFs. The observed changes in whole cell LRP1 steady state levels were further underlined

by cell surface biotinylation experiments. As expected, only mature LRP1-β is present on the cell surface. Inactivation of the NPxY2 endocytosis motif of LRP1 increases levels of LRP1-β on the cell surface compared to WT (Figure 5, right panel). Although there is a small pool of mature LRP1 in NPxY1 and NPxY1+2 mutant MEF cell lysates, mature LRP1-β cannot be detected on the cell surface. This further supports the hypothesis that NPxY1 and NPxY1+2 mutant mice closely resemble the complete LRP1 KO.
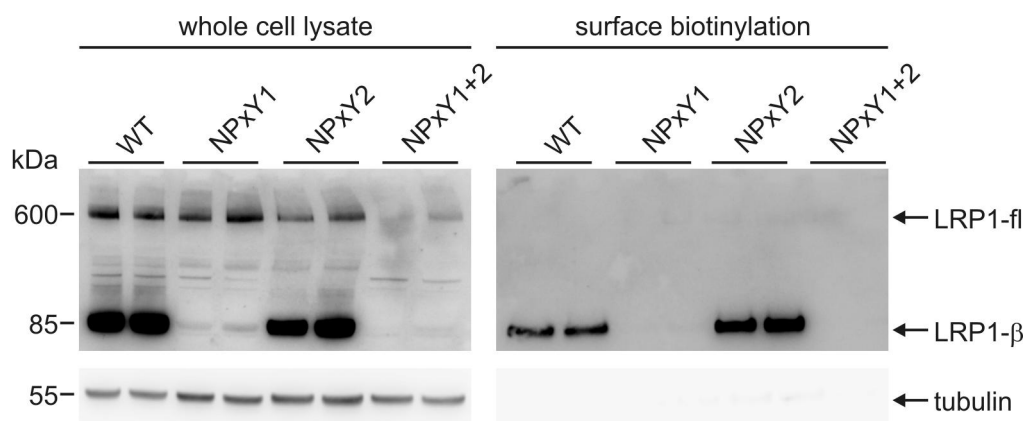
Figure 5   Low density lipoprotein receptor-related protein 1 (LRP1) knock-in mouse embryonic fibroblasts (MEFs) carrying the inactivated NPxY1 motif show impaired processing into mature LRP1-β and transport to the cell surface. Full-length (fl) immature LRP1 is present in all MEF cell lines whereas LRP1-β levels are severely reduced in MEFs carrying the NPxY1 inactivation (left panel). Cell surface biotinylation reveals that only the mature LRP1 receptor is present at the surface (right panel). Inactivation of the NPxY2 endocytosis motif increases cell surface expression of LRP1 compared to wild-type (WT). NPxY1 mutants do not reach the plasma membrane. LRP1-fl and LRP1-β were detected with 1704 antibody and tubulin was used as loading control.

3.2. NPxY1 and NPxY1+2 knock-in mutants show equal LRP1 production rates but a dramatically decreased half-life compared to WT LRP1

To investigate whether the reduced signal of mature LRP1 in the NPxY1 and NPxY1+2 mutants might be due to a reduced LRP1-fl production rate in the ER, we performed a 1 hour [^{35}S]-Met/Cys pulse labelling experiment. LRP1 immunoprecipitation and autoradiography did not show any obvious differences in the amounts of newly synthesised LRP1 in all MEF
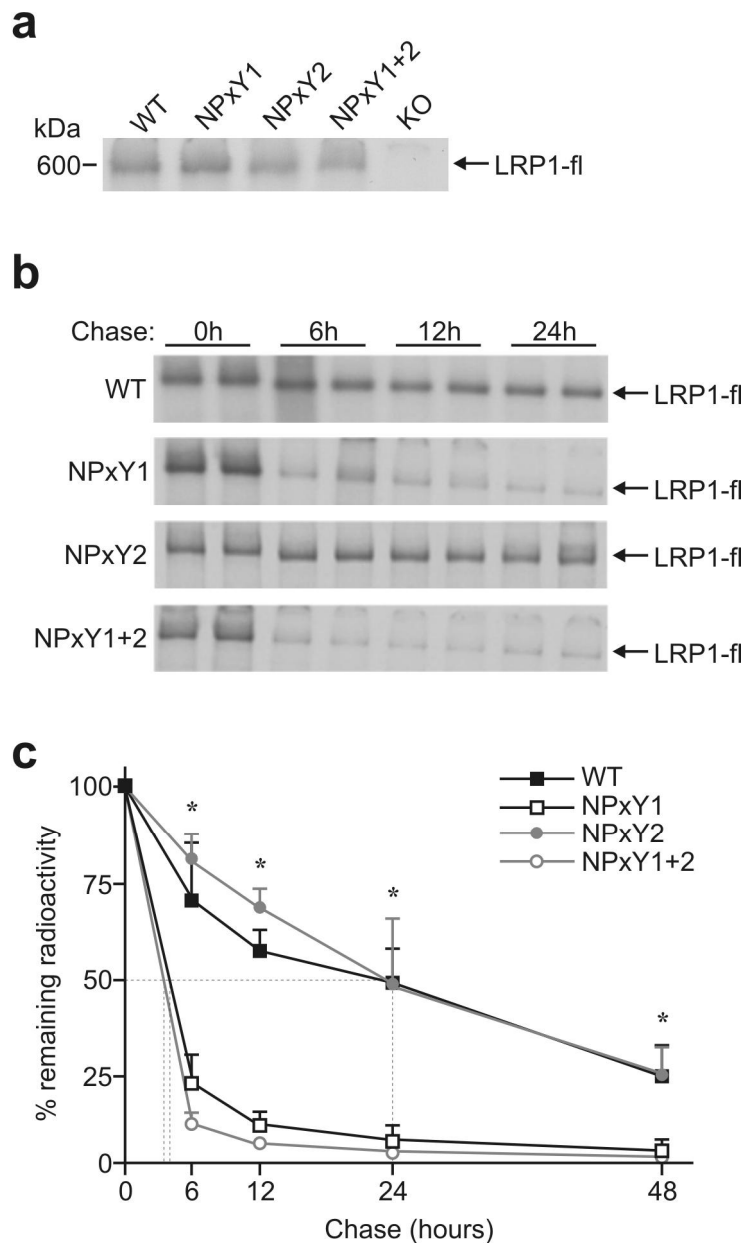
Figure 6 Full-length low density lipoprotein receptor-related protein 1 (LRP1-fl) rate of production is comparable in all cells but turnover is significantly increased in NPxY1 mutants compared to wild-type (WT). LRP1 knock-out (KO) MEFs were incorporated as negative control. (**a**) Autoradiography of LRP1-fl rate of production after a 1 hour metabolic [^{35}S] pulse labelling. (**b**) Autoradiography of immunoprecipitated LRP1-fl using the 1704 antibody at chase time points from 0 to 24 hours. (**c**) Half-life graph. Data are mean + SEM of three independent experiments. *Statistically significant difference ($p < 0.05$; t-test) between WT or NPxY2 with NPxY1 or NPxY1+2 is indicated.

cell lines (Figure 6a). Considering equal LRP1 production rates in all MEFs and reduced levels of mature LRP1 in NPxY1 and NPxY1+2 mutant MEFs we set out to determine the turnover of LRP1. Under physiologic conditions, LRP1-fl turnover occurs in the trans-Golgi by furin cleavage, resulting in mature LRP1. After pulse labelling for 1 hour, the cells were chased for different time points from 6, 12, 24 to 48 hours. During a 24 hour chase period,

LRP1-fl in WT and NPxY2 mutant MEFs was present at high levels, whereas NPxY1 and NPxY1+2 mutant LRP1-fl levels are dramatically decreased after 6 hours (Figure 6b). Determination of the half-life of LRP1-fl revealed a half-life of approximately 24 hours for WT and NPxY2 mutant LRP1 and of approximately 3.5 hours for NPxY1 and NPxY1+2 mutant LRP1 (Figure 6c). Although both NPxY1 mutant MEFs show an increased turnover of LRP1-fl compared to WT and the NPxY2 knock-in mutation, in whole cell lysates, barely any mature LRP1 can be detected (Figure 5, left panel).

3.3. NPxY1 and NPxY1+2 mutants show impaired transport to the trans-Golgi network

To unravel the paradox behind this impaired maturation and increased turnover of LRP1-fl in the NPxY1 and NPxY1+2 mutants, we interfered with the early secretory pathway to determine LRP1-fl routing within the cell. WT LRP1-fl is shuttled from the ER to the Golgi to undergo glycosylation and furin processing before the mature receptor is transported to the cell surface. MEF cell lines were incubated with brefeldin A (BFA), a compound that is known to disrupt transport from the ER to the Golgi network. BFA treatment resulted in an increase in LRP1-fl in all MEF cell lines regardless of any NPxY knock-in mutation by preventing LRP1 transport to the Golgi network (Figure 7a). Concomitantly, LRP1-β levels were reduced upon BFA treatment. Transport from medial to trans-Golgi compartments was blocked with monensin (Tartakoff, 1983). Monensin treatment increased LRP1-fl levels and decreased LRP1-β levels in WT and NPxY2 mutant MEFs by preventing transport to furin in the trans-Golgi compartment (Figure 7b). However, in NPxY1 and NPxY1+2 mutant MEFs it did not induce LRP1-fl accumulation. Taken together, this suggests that the prime cause of inefficient maturation of membrane proximal NPxY1 mutant LRP1 is upstream of receptor transport to late Golgi compartments.
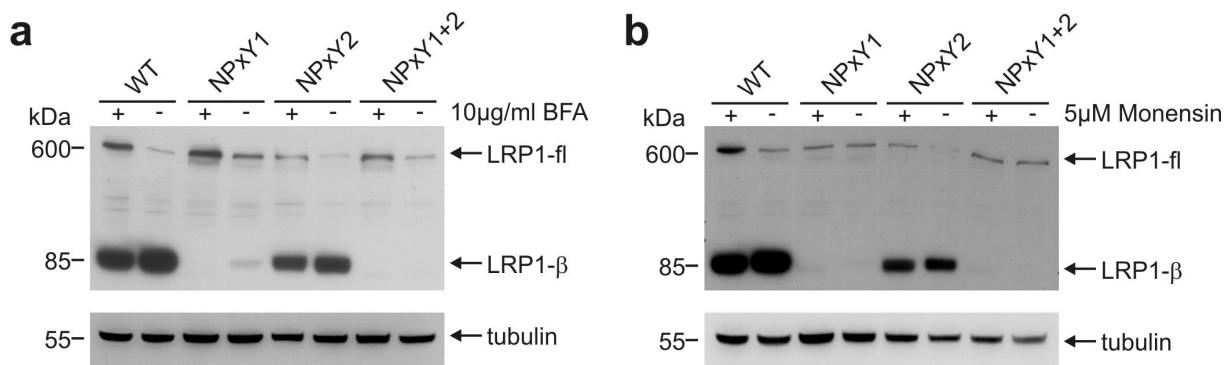
Figure 7 NPxY1 and NPxY1+2 mutant low density lipoprotein receptor-related protein 1 (LRP1) is not efficiently transported to the late Golgi compartments. (**a**) Full-length (fl) LRP1 is increased after Brefeldin A (BFA) treatment and LRP1-β is decreased. (**b**) Monensin treatment increases wild-type (WT) and NPxY2 mutant LRP1-fl levels, whereas NPxY1 and NPxY1+2 mutant LRP1-fl are not. LRP1 was detected with 1704 antibody after SDS-PAGE and Western blotting. α-tubulin was used as loading control.

3.4. NPxY1 inactivation results in premature proteasomal degradation of LRP1-fl

Since monensin treatment did not increase NPxY1 and NPxY1+2 mutant LRP1-fl levels, we analysed whether the proteasome degrades immature LRP1-fl before it reaches the trans-Golgi. We metabolically labelled all MEF cell lines for 1 hour in the presence or absence of MG132, an inhibitor of the proteasomal degradation pathway. Subsequently, cells were chased for 4 hours in normal growth medium with or without MG132. MG132 had only a minor effect on the levels of LRP1-fl in WT and NPxY2 mutant MEFs since the expression levels did not differ significantly between treated and untreated cells. However, MG132 treatment strongly increased LRP1-fl in NPxY1 and NPxY1+2 mutant MEFs (Figure 8a). Autoradiographic quantification of [^{35}S]-Met/Cys labelled LRP1-fl shows a significant increase in the ratio between treated and untreated MEFs containing the inactivated NPxY1 motif over both WT and NPxY2 mutant LRP1 (Figure 8b). This indicates that indeed a large portion of LRP1-fl is degraded by the proteasome in NPxY1 and NPxY1+2 MEFs before furin can generate the mature receptor.

3.5. LRP1 mutant MEF cell lines show decreased α$_2$-macroglobulin (α$_2$M) internalisation

Mature LRP1 on the cell surface functions as an endocytosis receptor. After ligand binding to
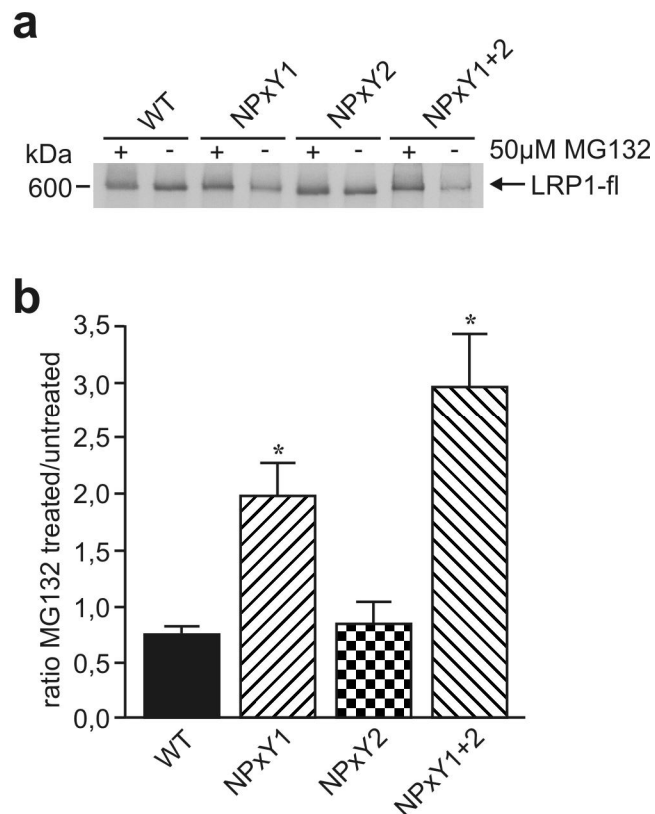
Figure 8 Immature low density lipoprotein receptor-related protein 1 (LRP1-fl) with the inactivated NPxY1 motif is degraded by the proteasome. (**a**) Autoradiography of immunoprecipitated LRP1-fl using the 1704 antibody after pulse/chase-labelling (1 and 4 hours respectively) in the presence (+) or absence (-) of 50 µM MG132. (**b**) The graph shows the impact of MG132 on LRP1-fl expression levels in comparison to untreated controls for each of the cell lines. Data are expressed as the ratio between treated and untreated controls and represent mean + SEM of three independent experiments. *Statistically significant difference ($p < 0.05$; ANOVA) compared to wild-type (WT) or NPxY2.

one of the four ligand binding domains of LRP1 the complex is internalised. To assess the function of NPxY mutant LRP1 as an endocytosis receptor, we investigated LRP1 specific uptake of iodinated α_2M in all MEF cell lines. Considering the varying levels of mature LRP1 on the cell surface, we plotted the data as ratio of internalised/surface bound α_2M. To reduce α_2M uptake in WT MEFs, receptor-associated protein (RAP) fused to glutathione S-transferase (GST) was used as ligand binding inhibitor. Internalisation of α_2M is significantly reduced in all NPxY mutant MEFs to background level observed in WT MEFs treated with RAP-GST (Figure 9).

In addition to α_2M, LRP1 has been shown to mediate endocytosis of more than 40 extracellular substrates (Dieckmann et al.). Among them is the key pathogen involved in Alzheimer's disease development, the amyloid-β (Aβ) peptide. Furthermore, it was shown

that LRP1 mediates Aβ clearance from brain-to-blood across the blood-brain barrier (BBB) by a transcytotic mechanism (Shibata et al., 2000). Due to the embryonic lethal phenotype of LRP1 KO animals this study was based on ligand binding inhibition approaches, e.g. by RAP. Since we observed a reduced LRP1 endocytosis rate in NPxY2 mutant MEFs derived from the viable LRP1 NPxY2 knock-in mouse, we set out to provide genetic evidence for LRP1-mediated Aβ transcytosis across the BBB. Our approach is based on the establishment of an *in vitro* BBB transport model, consisting of primary endothelial cells generated from WT and NPxY2 mutant mice, and is described in the following sections.
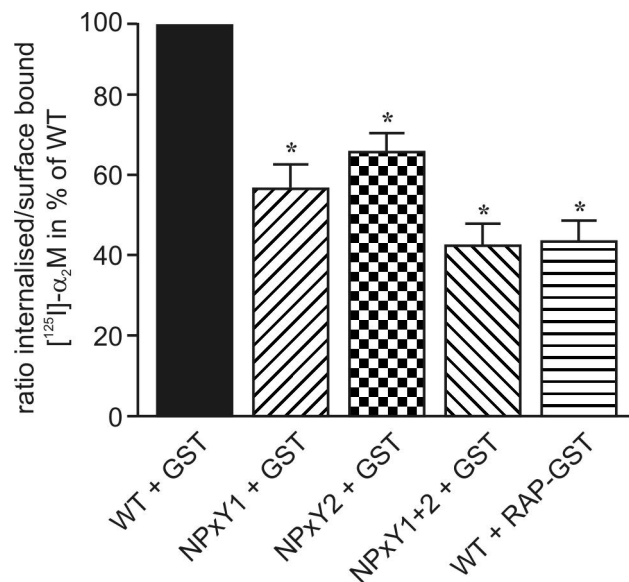
Figure 9   Functionality of the mature low density lipoprotein receptor-related protein 1 (LRP1) receptor in mouse embryonic fibroblast (MEF) cell lines was analysed by a α_2-macroglobulin (α_2M) endocytosis assay. RAP-GST reduces endocytosis of activated [^{125}I]-α_2M in wild-type (WT) LRP1 MEFs compared to GST control. All LRP1 knock-in mutants show decreased α_2M internalisation compared to WT MEFs. Results represent mean + SEM of 2 independent experiments performed in duplicates. *Statistically significant difference ($p < 0.05$; ANOVA) compared to WT + GST.

3.6. Primary mouse brain capillary endothelial cells (pMBCECs) represent a suitable *in vitro* BBB model to conduct transport studies

In addition to astrocytes and pericytes, endothelial cells (ECs) establish the BBB. ECs are characterised by a flattened spindle-shaped morphology and, at the BBB, they limit paracellular diffusion by forming a tight EC barrier. To address the question whether

pMBCECs mimic BBB properties *in vitro*, we examined their ability to form a tight endothelial monolayer with BBB specific characteristics. After isolation of pMBCECs, capillary fragments were plated into collagenIV/fibronectin coated dishes (Figure 10a). By day *in vitro* (DIV) 1, ECs adhered to the matrix and started to migrate out of the vessel fragment (Figure 10b). At DIV 3 the vessel fragment is converted into a cell patch (Figure 10c), whereupon ECs of all cell patches proliferate to form a confluent monolayer by DIV 6 with the EC specific spindle-shaped phenotypic morphology (Figure 10d). Furthermore, we analysed the expression of tight junction (TJ) proteins in our pMBCEC cultures and found strong expression of TJ specific proteins occludin and ZO-1 by confocal microscopy (Figure 10e and f). Since transendothelial electrical resistance (TEER) is regarded as a measure of barrier integrity, we also investigated TEER levels of pMBCECs cultured on transwell inserts (Figure 4). After withdrawing serum and adding physiologic concentrations of hydrocortisone (HC; 550 nM) for 24 hours we were able to significantly increase TEER values from $195,8 \pm 13,3 \ \Omega cm^2$ to $316,2 \pm 24,9 \ \Omega cm^2$ (Figure 10g).

3.7. LRP1 is expressed in pMBCECs

Although genetic evidence is missing due to the embryonic lethal phenotype of LRP1 KO mice, LRP1 has been described to mediate Aβ clearance from the brain into the blood across the BBB by means of transcytosis (Herz et al., 1992; Shibata et al., 2000). Therefore, we examined LRP1 protein expression by Western blot analysis in freshly isolated pMBCECs and found a good expression of the LRP1-β subunit, representing the membrane bound subunit of the mature receptor (Figure 11a). In addition, 24 hours after induction of high TEER, at the stage when cultured pMBCECs were used for transport studies, we investigated the functionality of LRP1 in pMBCECs with regard to its endocytosis capability of its ligand
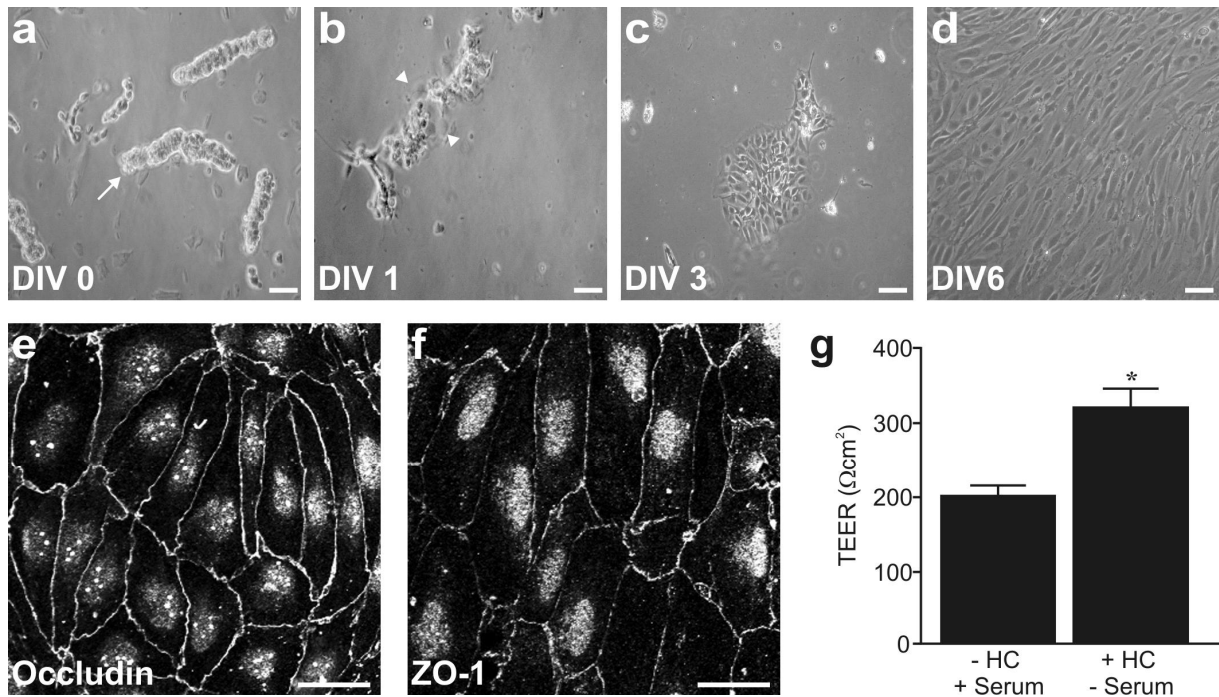
Figure 10 Primary mouse brain capillary endothelial cells (pMBCECs) are a suitable model of the blood-brain barrier (BBB) to conduct transport studies. Freshly isolated pMBCECs were cultured on collagen IV/fibronectin coated dishes for 5 days before serum was withdrawn and 550 nM hydrocortisone (HC) was added for 24 hours to study the BBB phenotype *in vitro*. (**a-d**) Differential interference contrast images of pMBCECs at several days *in vitro* (DIV). Arrow in DIV 0 image points at typical vessel fragment (**a**) and arrowhead in DIV 1 image indicates outgrowing endothelial cells (**b**). By DIV 3 the initial vessel fragment appears as cell patch (**c**) whereas the confluent pMBCEC monolayer at DIV 6 shows the typical spindle-shaped morphology of endothelial cells (**d**). (**e** and **f**) pMBCECs express tight junction proteins occludin (**e**) and ZO-1 (**f**) as analysed by immunofluorescence. (**g**) HC induces high transendothelial electrical resistance (TEER) in confluent pMBCEC monolayers cultured on permeable 6-well transwell cell culture inserts. Results represent mean + SEM of 25 independent experiments. *Statistically significant difference ($p < 0.05$; t-test) between pMBCECs without HC and 24 hours after addition of HC. Scale bar 50µm.

α_2M. In an endocytosis assay, we analysed the ratio of internalised to cell surface bound activated [^{125}I]-α_2M as a measure of uptake. Uptake of radiolabelled α_2M by pMBCECs was significantly reduced by addition of RAP-GST, an LRP1 ligand binding inhibitor, when compared to the addition of GST alone (Figure 11b).

Receptor for advanced glycation end products (RAGE) has been described to be the main transmembrane receptor involved in Aβ transport from blood-to-brain (Deane et al., 2003). However, in contrast to rat lung tissue, in pMBCECs we could not detect RAGE protein expression (Figure 11a). Therefore, in our transport assays we focussed on LRP1-mediated Aβ transcytosis.
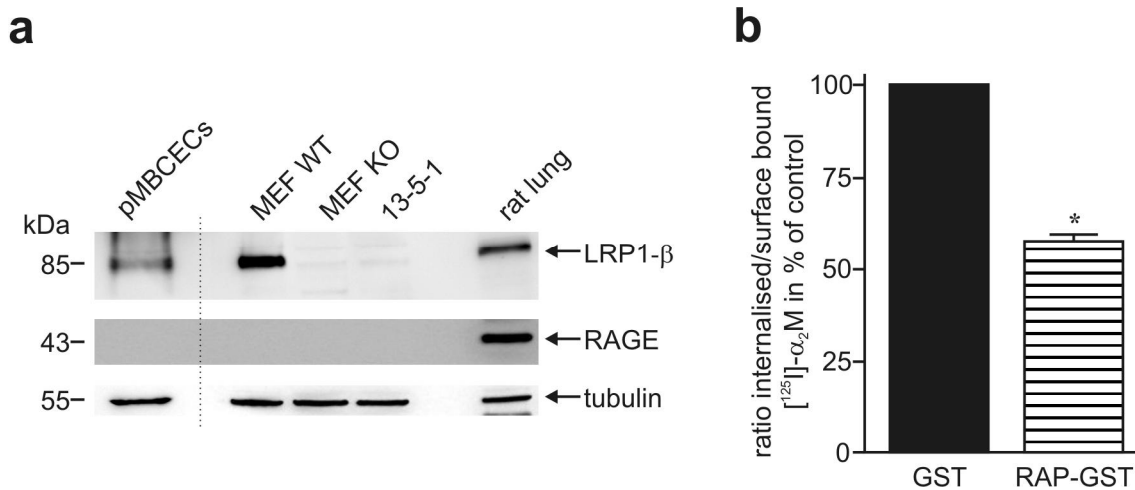
Figure 11 Primary mouse brain capillary endothelial cells (pMBCECs) express the low density lipoprotein receptor-related protein 1 (LRP1) but not the receptor for advanced glycation end products (RAGE). (**a**) Detection of the mature LRP1-β subunit in freshly isolated pMBCECs, mouse embryonic fibroblast (MEF) cell lines expressing LRP1 (WT) and deficient in LRP1 (KO), LRP1-deficient CHOs (13-5-1) and rat lung tissue by Western blot analysis using rabbit polyclonal anti-LRP1 antibody (1704). RAGE expression was analysed with goat anti-RAGE specific IgG. A mouse monoclonal anti-tubulin antibody was used as loading control. (**b**) Functionality of the mature LRP1 receptor on pMBCECs cultured for 6 days *in vitro* was analysed by a α_2-macroglobulin (α_2M) endocytosis assay. RAP-GST reduces endocytosis of activated $[^{125}I]$-α_2M in pMBCECs compared to GST control. Results represent mean + SEM of 3 independent experiments. *Statistically significant difference ($p < 0.05$; t-test) between pMBCECs treated with RAP-GST or GST.

3.8. Integrity of $[^{125}I]$-Aβ 1-40 (Aβ_{1-40})

Our next aim was to determine the stability of commercial $[^{125}I]$-Aβ_{1-40} under the conditions used during the transcytosis experiments. Trichloroacetic acid (TCA) precipitation of media samples containing 0.1 nM $[^{125}I]$-Aβ_{1-40} enabled us to differentiate between intact $[^{125}I]$-Aβ_{1-40} and free $[^{125}I]$ (non TCA-precipitable). The experiments revealed a minor disintegration of $[^{125}I]$ from $[^{125}I]$-Aβ_{1-40} during the 6 hour time course as shown by the decrease in $[^{125}I]$-Aβ_{1-40} counts and the concomitant increase in $[^{125}I]$ counts (Figure 12a and b). Furthermore, autoradiography of media samples separated on a 16% bis-tris gel also showed a minor decrease in $[^{125}I]$-Aβ_{1-40} during 6 hours whereas no appearance of Aβ dimers or higher oligomers was detected (Figure 12c). Dimerisation of Aβ is of particular importance because they have been described to be less efficiently transported by LRP1 (Ito et al., 2007). Hence, in further experiments we only considered TCA precipitated intact $[^{125}I]$-Aβ_{1-40} to calculate the Aβ_{1-40} transcytosis quotient (TQ).
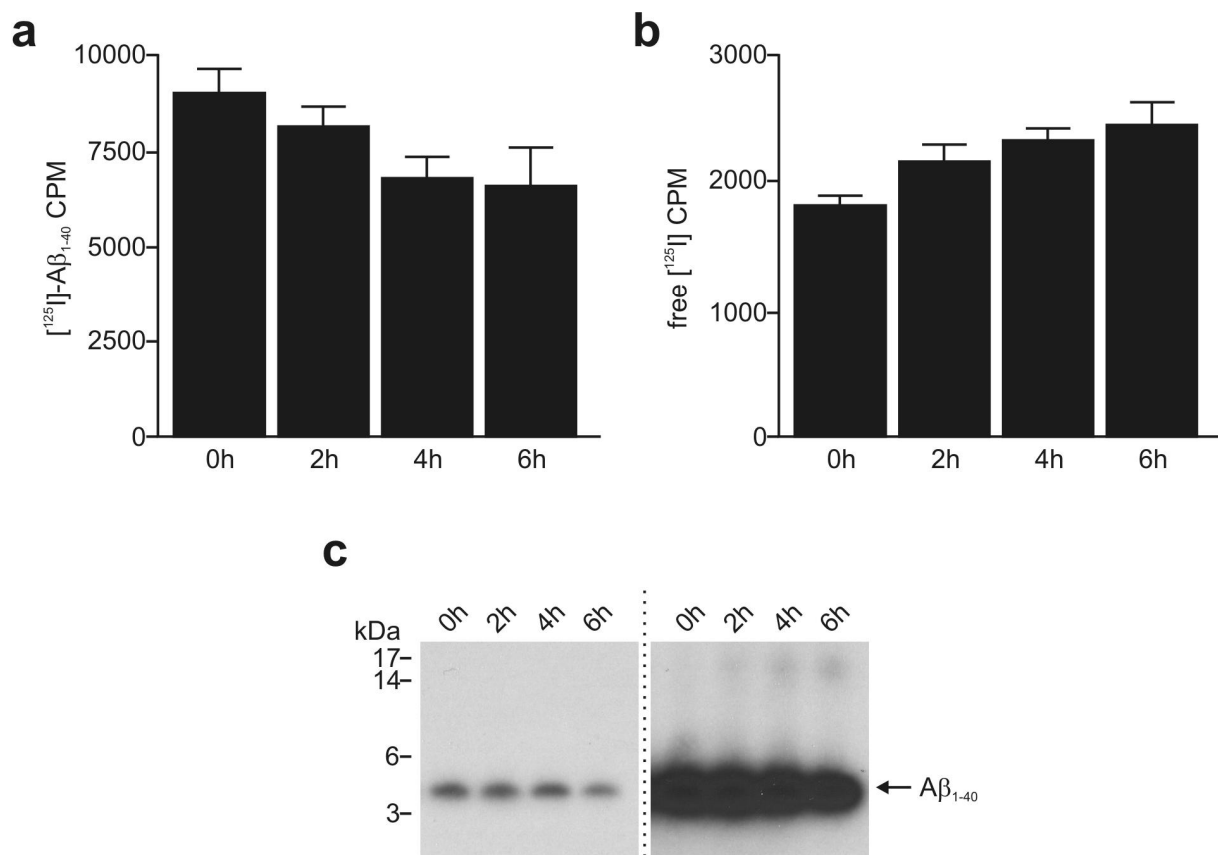
Figure 12 Only a small amount of [^{125}I] spontaneously disintegrates from [^{125}I]-amyloid-β 1-40 (Aβ$_{1-40}$) whereas no Aβ dimers are formed within 6 hour incubation. (**a** and **b**) 0.1nM [^{125}I]-Aβ$_{1-40}$ was incubated in medium at 37 °C before samples were subjected to trichloroacetic acid precipitation. Intact [^{125}I]-Aβ$_{1-40}$ and free [^{125}I] counts per minute (CPM) were analysed separately on a γ-counter. A minor disintegration of [^{125}I] from [^{125}I]-Aβ$_{1-40}$ during the 6 hour time course is shown by the decrease in [^{125}I]-Aβ$_{1-40}$ CPM (**a**) and the concomitant increase in [^{125}I] CPM (**b**). Results are expressed as mean + SEM of three independent experiments. (**c**) Dimerisation of [^{125}I]-Aβ$_{1-40}$ was investigated for up to 6 hours. Samples were separated on a 16% bis-tris gel and the results were visualised by autoradiography. Left panel shows a short exposure and right panel a long exposure. A decrease in [^{125}I]-Aβ$_{1-40}$ monomers (arrow) during the 6 hour incubation time was detected whereas no formation of dimers was found.

3.9. LRP1 is a receptor for bidirectional transcytosis of Aβ$_{1-40}$ across the *in vitro* BBB model

LRP1 has so far been described to mediate Aβ clearance from brain-to-blood (Shibata et al., 2000). Therefore, in a first set of experiments, we investigated the transport of [^{125}I]-Aβ$_{1-40}$ from the abluminal to luminal direction (brain-to-blood) across pMBCEC monolayers grown

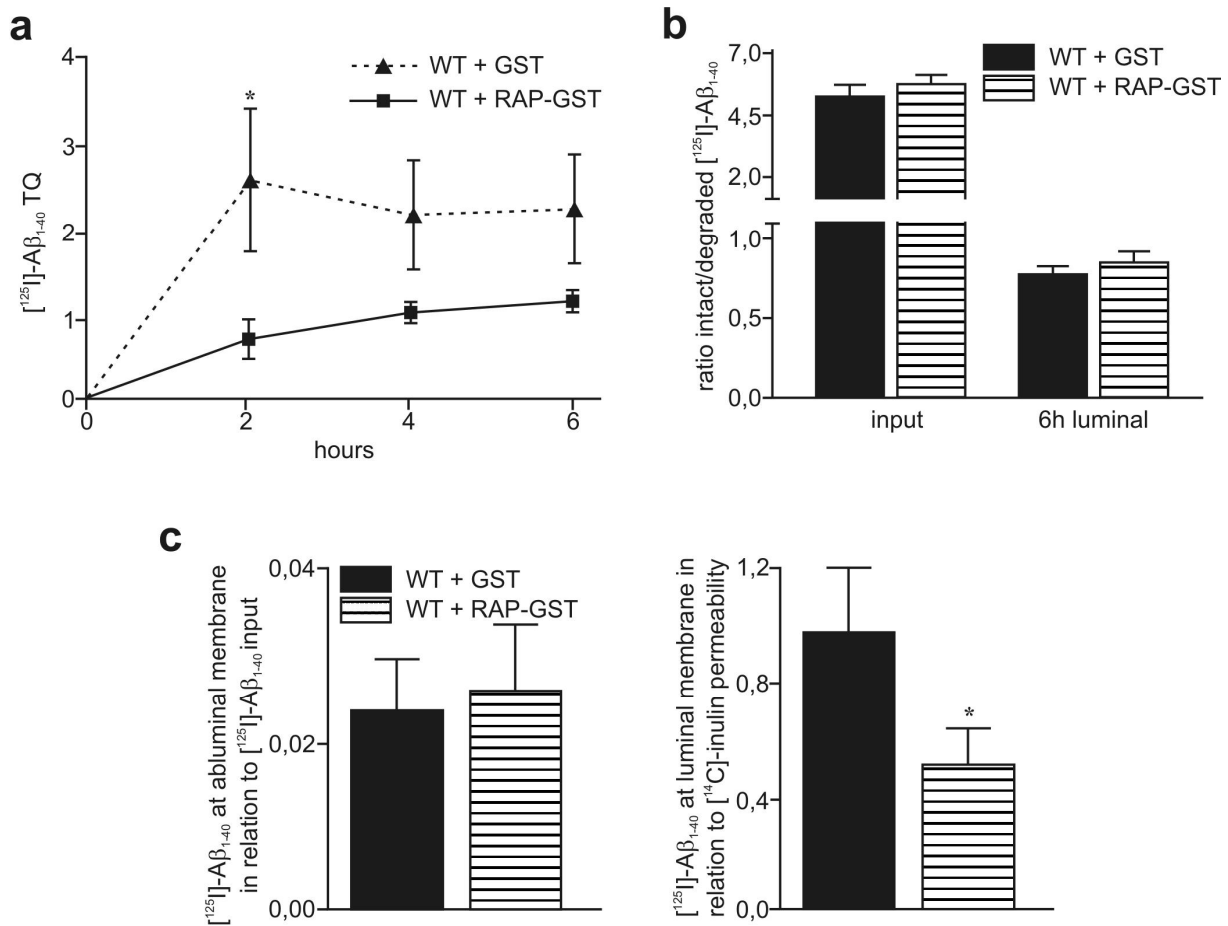**Figure 13** Low density lipoprotein receptor-related protein 1 (LRP1) transcytoses amyloid-β 1-40 (Aβ$_{1-40}$) from brain-to-blood. Freshly isolated primary mouse brain capillary endothelial cells (pMBCECs) were cultured on collagen IV/fibronectin coated transwell inserts for 5 days before high transendothelial electrical resistance was induced for 24 hours by serum withdrawal and addition of hydrocortisone. Subsequently, transport studies for [^{125}I]-Aβ$_{1-40}$ were conducted in the presence of [^{14}C]-inulin as a marker for paracellular diffusion. Results represent mean ± SEM of 3 independent experiments. *Statistically significant difference (*p* < 0.05; t-test). (**a**) pMBCECs cultured on 6-well transwell inserts were analysed for LRP1-mediated transport of [^{125}I]-Aβ$_{1-40}$ from the abluminal to luminal compartment (brain-to-blood) over a 6 hour time period. RAP-GST decreases the transport rate of [^{125}I]-Aβ$_{1-40}$ to the luminal compartment at each time point compared to GST control. (**b**) Analysis of the ratios of intact versus degraded [^{125}I]-Aβ$_{1-40}$ in the luminal acceptor compartment after 6 hour transport revealed no effect of RAP-GST on LRP1-mediated degradation of [^{125}I]-Aβ$_{1-40}$ compared to GST. (**c**) Surface bound [^{125}I]-Aβ$_{1-40}$ at the abluminal (left panel) and luminal (right panel) membrane of pMBCECs cultured in 24-well transwell inserts. Fifteen minutes after addition of [^{125}I]-Aβ$_{1-40}$ to the abluminal compartment, surface bound proteins were dissociated by acidic washes and subjected to analysis. RAP-GST did not decrease binding of [^{125}I]-Aβ$_{1-40}$ to the abluminal membrane (left panel), though, the amount of radiolabelled Aβ$_{1-40}$ transcytosed from the abluminal to luminal membrane was reduced by RAP-GST (right panel).

on 6-well transwell filters over a 6 hour time period. We determined the TQ as:

$$\text{A}\beta_{1\text{-}40} \text{ TQ} = \frac{([^{125}I]-A\beta_{1-40})_{acceptor}\big/([^{125}I]-A\beta_{1-40})_{input}}{([^{14}C]-inulin)_{acceptor}\big/([^{14}C]-inulin)_{input}}$$. Inulin was added as a marker for

paracellular leakage and, therefore, can be regarded as internal control for barrier tightness.

The lower compartment of transwell dishes resembles the abluminal (brain) side and the

upper compartment the luminal (blood) side. In our experimental set up, RAP-GST inhibited transport of iodinated $A\beta_{1-40}$ from brain-to-blood at each time point (Figure 13a). After TCA precipitation of media samples we were able to distinguish intact $[^{125}I]$-$A\beta_{1-40}$ from free $[^{125}I]$ (non TCA-precipitable, generated during $[^{125}I]$-$A\beta_{1-40}$ degradation by pMBCECs or spontaneous $[^{125}I]$ disintegration). Analysis of the ratios of intact versus degraded $[^{125}I]$-$A\beta_{1-40}$ revealed no differences in the input. Interestingly, after 6 hour transport there was no difference in the ratio of intact versus degraded $[^{125}I]$-$A\beta_{1-40}$ in the luminal acceptor compartment for RAP-GST compared to GST control (Figure 13b). Hence, we hypothesise that LRP1 might not participate in the degradation of $[^{125}I]$-$A\beta_{1-40}$ during transcytosis as recently suggested in a study investigating $A\beta$ transport across an epithelial monolayer (Nazer et al., 2008). In surface binding studies, we determined the amount of intact $[^{125}I]$-$A\beta_{1-40}$
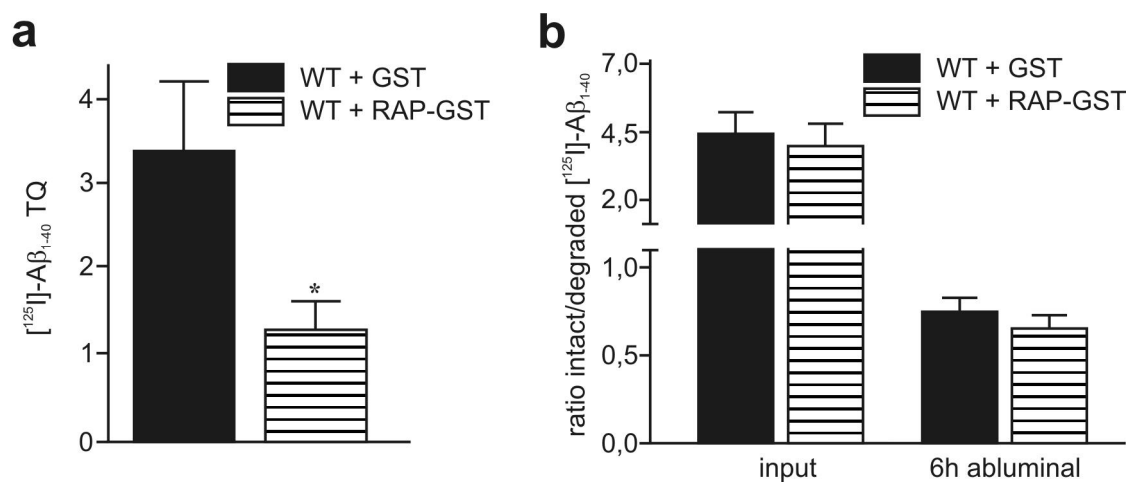
Figure 14 Low density lipoprotein receptor-related protein 1 (LRP1) transcytoses amyloid-β 1-40 ($A\beta_{1-40}$) in the blood-to-brain direction across primary mouse brain capillary endothelial cell (pMBCEC) monolayers. Transport studies for $[^{125}I]$-$A\beta_{1-40}$ were performed in the presence of $[^{14}C]$-inulin (a marker for paracellular diffusion) after inducing high transendothelial electrical resistance. Results represent mean + SEM of 3 independent experiments. *Statistically significant difference ($p < 0.05$; t-test). (**a**) pMBCECs cultured on 24-well transwell inserts were analysed for LRP1-mediated transport of $[^{125}I]$-$A\beta_{1-40}$ from the luminal to abluminal compartment (blood-to-brain). After 6 hours, RAP-GST treated monolayers showed a reduction in $[^{125}I]$-$A\beta_{1-40}$ transport from blood-to-brain compared to GST control. (**b**) Ratios of intact versus degraded $[^{125}I]$-$A\beta_{1-40}$ in the abluminal acceptor compartment after 6 hour transport show no effect of RAP-GST on $[^{125}I]$-$A\beta_{1-40}$ degradation compared to GST.

bound to the plasma membrane of pMBCECs cultured in 24-well transwell dishes. After incubation of pMBCECs with radiolabelled $A\beta_{1-40}$ in the abluminal compartment for 15

minutes, we found no difference in binding of $[^{125}I]$-A$\beta_{1\text{-}40}$ to the abluminal membrane when RAP-GST or GST were present. However, the amount of $[^{125}I]$-A$\beta_{1\text{-}40}$ transcytosed from the abluminal to luminal membrane was significantly reduced by approximately 50% with RAP-GST compared to GST control, indicating that LRP1 acts as the transcytosis receptor (Figure 13c).

RAGE is the only described transmembrane protein mediating Aβ transport from blood-to-brain (Deane et al., 2003). In our analyses we could not show RAGE in pMBCECs (Figure 11). Due to the fact that we could not detect a significant increase in LRP1-mediated transcytosis of $[^{125}I]$-A$\beta_{1\text{-}40}$ from brain-to-blood after 2 hour incubation periods, we also investigated Aβ transcytosis from blood-to-brain. We detected a statistically significant LRP1-mediated transport of $[^{125}I]$-A$\beta_{1\text{-}40}$ from the luminal to abluminal compartment (blood-to-brain). RAP-GST reduced the $[^{125}I]$-A$\beta_{1\text{-}40}$ transport within 6 hours by approximately 50% compared to control (Figure 14a). Further, we were not able to detect a difference in the ratios of intact versus degraded $[^{125}I]$-A$\beta_{1\text{-}40}$ in the abluminal acceptor compartment for RAP-GST compared to GST control, again providing further evidence that LRP1 is rather participating in Aβ transcytosis than lysosomal degradation of Aβ in pMBCECs (Figure 14b).

3.10. NPxY2 mutant pMBCECs transcytose less A$\beta_{1\text{-}40}$

To provide genetic evidence for LRP1-mediated transcytosis of $[^{125}I]$-A$\beta_{1\text{-}40}$ across the BBB, we performed a 2 hour transport study across pMBCEC monolayers derived from LRP1 NPxY2 knock-in mice versus WT control littermate pMBCECs. As described above, NPxY2 mutant MEFs showed reduced α_2M endocytosis (Figure 9). Brain-to-blood transport of iodinated A$\beta_{1\text{-}40}$ was significantly reduced by approximately 50% in NPxY2 mutant pMBCECs compared to WT monolayers (Figure 15a). This result provides for the first time genetic proof for an involvement of LRP1 in Aβ transcytosis across the BBB, since we could not detect a difference in the ratio of intact versus degraded $[^{125}I]$-A$\beta_{1\text{-}40}$ in the luminal

compartment after 2 hour transport when NPxY2 monolayers were compared to WT pMBCECs (Figure 15b). Furthermore, NPxY2 mutant monolayers also showed an impaired transcytosis capability for $[^{125}I]$-Aβ_{1-40} in the blood-to-brain direction compared to WT pMBCECs (Figure 15c).
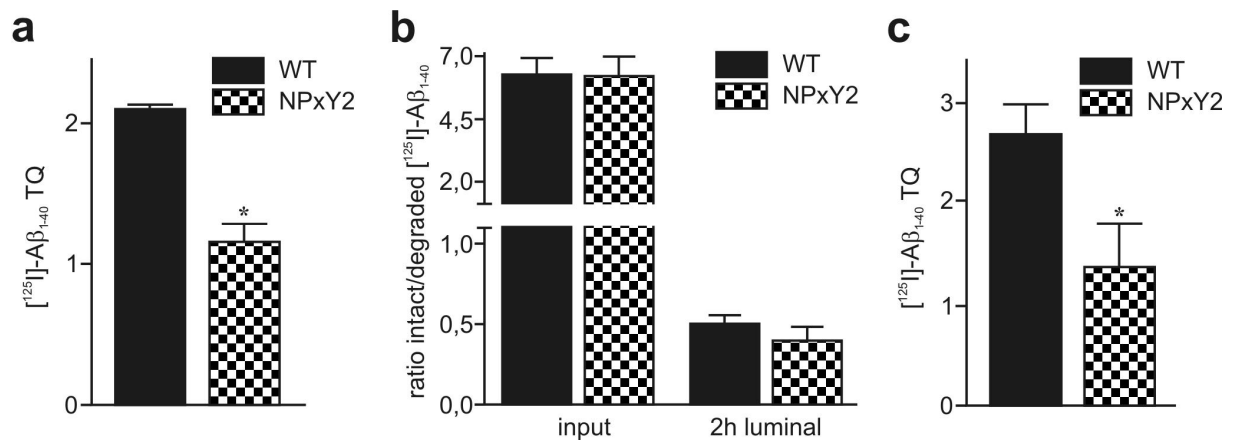
Figure 15 Low density lipoprotein receptor-related protein 1 (LRP1) carrying a mutation in the NPxY2 domain transcytoses less amyloid-β 1-40 (Aβ$_{1-40}$) across primary mouse brain capillary endothelial cell (pMBCEC) monolayers. Results represent mean + SEM of 3 independent experiments. (**a**) Transcytosis of $[^{125}I]$-Aβ$_{1-40}$ across WT and NPxY2 mutant pMBCECs cultured on 24-well transwell inserts was analysed for 2 hours in the brain-to-blood direction. NPxY2 monolayers showed a reduction in $[^{125}I]$-Aβ$_{1-40}$ transport from brain-to-blood compared to WT control littermate derived pMBCECs. (**b**) Analysis of the ratios of intact versus degraded $[^{125}I]$-Aβ$_{1-40}$ in the luminal acceptor compartment after 2 hour transport shows no difference in $[^{125}I]$-Aβ$_{1-40}$ degradation during transcytosis between NPxY2 mutant and WT derived pMBCECs. (**c**) $[^{125}I]$-Aβ$_{1-40}$ transcytosis across WT and NPxY2 mutant pMBCECs cultured on 24-well transwell inserts was analysed for 6 hours in the blood-to-brain direction. NPxY2 monolayers showed a reduction in $[^{125}I]$-Aβ$_{1-40}$ transport from blood-to-brain compared to WT pMBCECs. *Statistically significant difference ($p < 0.05$; t-test).

4. DISCUSSION

4.1. Inactivation of the proximal NPxY motif impairs early steps in low density lipoprotein receptor-related protein 1 (LRP1) biosynthesis

Due to the early embryonic lethal phenotype of LRP1 knock-out (KO) mice, most studies on LRP1 function have been limited to LRP1 overexpression studies with truncated LRP1 mini-receptors *in vitro* (Herz et al., 1992). To gain more information about the function of endogenous LRP1, Roebroek and colleagues generated LRP1 knock-in mice by recombinase-mediated cassette exchange (RMCE) to modify the endogenous LRP1 gene. Alanine (A) subsititutions within the NPxY domains (NPxY → AAxA) caused distinct phenotypes in LRP1 knock-in mice (Reekmans et al., 2009; Roebroek et al., 2006). Whereas the viable and fertile NPxY2 mutant mouse does not show any obvious phenotype, inactivation of the membrane proximal NPxY1 motif or a combined NPxY1+2 mutation resulted in embryonic to perinatal lethality. The absence of an obvious phenotype in the NPxY2 mutant mouse could be explained by assuming that the NPxY2 motif is not essential for some functions of LRP1. An alternative explanation is that the NPxY1 motif can compensate for the lack of the NPxY2 motif, because of the postulated significance of the NPxY2 motif in e.g. interaction with adaptor proteins. Given the embryonic lethal phenotype of NPxY1 mutant mice, such compensatory mechanism can not be provided by the NPxY2 motif in case of NPxY1 mutation. Combined inactivation of both NPxY motifs (NPxY1+2) resulted in an earlier embryonic lethal phenotype as the single inactivation of the proximal NPxY1 domain (Reekmans et al., 2009; Roebroek et al., 2006). It can be hypothesised that the additional inactivation of NPxY2 is responsible for this earlier lethal phenotype. Possibly, the NPxY2 domain is only partly able to complement for the loss of the NPxY1 domain, shifting embryonic lethality towards a later stage of development in the NPxY1 mutant compared to the NPxY1+2 mutant. The observed lethal phenotype within a broad developmental window of embryonic day (E) 10.5 to E 13.5 of the double mutant seems not to be much different

from the full LRP1 KO allele (Herz et al., 1992). Here, we analysed mouse embryonic fibroblasts (MEFs) generated from LRP1 knock-in mice for LRP1 receptor maturation and function to elucidate why NPxY1 mutant mice closely mimick the complete LRP1 KO.

Cell biological analyses of the different MEFs, which were derived from the several LRP1 knock-in embryos, confirm the almost complete loss of mature LRP1 in NPxY1 and NPxY1+2 mutant MEFs (Figure 5). In agreement with the viable phenotype of the LRP1 NPxY2 knock-in mouse, MEFs carrying the mutated NPxY2 motif showed normal steady state levels of mature LRP1 compared to wild-type (WT) MEFs. Analysis of full-length (fl) immature LRP1 synthesis in all NPxY mutant MEFs revealed no differences in production rate compared to WT MEFs indicating no transcriptional abnormalities due to the genetic modifications (Figure 6a). In addition, determination of the half-life of LRP1-fl in pulse chase experiments gave us a direct measure of LRP1-fl stability within the cell and, eventually its processing into mature LRP1. Due to comparable LRP1-fl production rates in all LRP1 mutant MEFs and, the reduced amount of mature LRP1 in NPxY1 and NPxY1+2 mutant MEFs, it can be speculated that LRP1-fl accumulates in NPxY1 and NPxY1+2 mutant cells if LRP1 is not processed by furin into the mature receptor. However, pulse chase experiments revealed a tremendously shorter LRP1-fl half-life in NPxY1 and NPxY1+2 mutant MEFs compared to WT and NPxY2 cells (Figure 6b and c). However, steady state levels of the β-subunit, representative for mature LRP1, on the contrary, are severely reduced in the NPxY1 and NPxY1+2 mutants and fail to reach the cell surface (Figure 5). The mechanism underlying these observations reflects either altered transport of LRP1 along the secretory pathway to the cell surface or altered subsequent internalisation to endosomal/lysosomal compartments. Therefore, we first focussed on LRP1 transport within the secretory pathway to investigate a possibly modified processing of the different LRP1 mutants.

To gain further insight into LRP1-fl routing throughout the secretory pathway we interfered with the secretory pathway by using brefeldin A (BFA) and monensin. BFA interrupts exit

from the endoplasmatic reticulum (ER) and, moreover, transport from ER to the Golgi where immature LRP1-fl is processed by furin into the mature receptor (Willnow et al., 1996). Treatment with BFA increased LRP1-fl levels in WT and all NPxY mutant MEFs, whereas mature LRP1 levels decreased in the presence of BFA (Figure 7a). LRP1-fl accumulation in the ER upon BFA treatment shows that LRP1 mRNA is still translated while ER exit is blocked. This indicates that LRP1 translation at ER residing ribosomes is not altered by the introduced genetic substitutions. Therefore, we hypothesised that LRP1 transport to the late Golgi, where furin generates mature LRP1, is impaired. MEF treatment with monensin, which blocks transport from early to late Golgi compartments, increased LRP1-fl levels in WT and NPxY2 mutant MEFs but it failed to increase LRP1-fl in NPxY1 and NPxY1+2 mutant MEFs (Figure 7b). Taken together, this suggests that the majority of LRP1-fl in NPxY1 and NPxY1+2 mutant MEFs is unable to reach late Golgi compartments, where furin cleavage of LRP1 occurs, but also that LRP1-fl must exit the secretory pathway. Most likely, this exit results in premature degradation of LRP1-fl in NPxY1 and NPxY1+2 mutant MEFs.

The proteasome is a cellular component involved in protein degradation. To analyse a potential premature proteasomal degradation of LRP1-fl in NPxY1 and NPxY1+2 mutant MEFs, we blocked the proteasome with MG132. In our experimental set up, proteasome inhibition was performed in pulse chase experiments to track newly synthesised LRP1-fl in all MEFs over a defined time period. Cells were pulse labelled for 1 hour in the presence of MG132 or solvent control and subsequently chased for 4 hours with or without MG132. Autoradiographic analysis shows that LRP1-fl levels are increased in NPxY1 and NPxY1+2 mutant MEFs when the proteasome was blocked whereas there was no significant effect of MG132 on WT or NPxY2 mutant LRP1-fl levels (Figure 8). Hence, we were able to show that LRP1-fl in NPxY1 and NPxY1+2 mutant MEFs is prematurely degraded by the proteasome before it reaches the trans-Golgi compartment where mature LRP1 is generated.

Finally, in order to investigate the function of mature cell surface LRP1 as a receptor for ligand endocytosis in our NPxY mutant MEFs, we analysed LRP1-mediated α_2-macroglobulin (α_2M) uptake in an internalisation assay. The involvement of the proximal NPxY1 and distal NPxY2 motifs in basolateral sorting, internalisation and recycling was revealed by overexpression studies of LRP1 mini-receptors with a strongly in size reduced α-subunit and mutants thereof (Li et al., 2000; Marzolo et al., 2003; van Kerkhof et al., 2005). In these exogenous overexpression analyses, mutants defective in endocytosis containing a tyrosine mutation within the NPxY2 motif accumulated more at the cell surface compared to WT. This is in agreement with our cell surface biotinylation experiments showing that NPxY2 mutant LRP1 accumulates on the cell surface compared to WT LRP1 (Figure 5). In the present study we also show that the endogenous levels of NPxY1 and NPxY1+2 mutant MEFs reveal strongly reduced mature LRP1 levels and an absence of mature LRP1 on the cell surface due to premature proteasomal degradation of LRP1-fl (Figure 5 and 8). Increased cell surface levels of mature LRP1 in NPxY2 mutant MEFs are indirectly displayed in our α_2M uptake assay. Compared to WT MEFs, NPxY2 mutant MEFs internalise significantly less α_2M due to the mutated endocytosis motif (Figure 9). α_2M internalisation by WT LRP1 was blocked with RAP-GST to background levels. As expected, NPxY1 and NPxY1+2 MEFs lacking mature LRP1 on the cell surface showed background α_2M internalisation comparable with WT MEFs treated with RAP-GST.

Due to the difference in expression systems i.e. exogenous versus endogenous expression levels and/or due to differences in protein context i.e. mini-LRP1 versus LRP1-fl, different aspects of the role of particular motifs in the LRP1 intracellular domain are disclosed. Potentially, the exogenous expression levels of LRP1 mini-receptors are sufficient to overcome premature degradation in adequate amounts, thereby, allowing analyses of the functional significance of NPxY1 and NPxY2 motifs near the cell surface. In fact, differences in premature degradation might be masked in this setting. The novel finding of the present

study is that especially the NPxY1 motif of LRP1 is essential for early sorting steps in the ER/early Golgi, preceding the generation of mature LRP1. It might be of great interest to investigate whether other lipoprotein receptors that share the overall C-terminal structure with two neighbouring NPxY domains show similar effects. The importance of the distal NPxY2 motif in receptor internalisation is displayed by increased cell surface levels of mature LRP1 compared to WT and, reduced α_2M internalisation (Figure 5 and 9). The lack of phenotype in LRP1 NPxY2 mutant mice and their derived MEFs argue against an important role of this motif in early sorting steps in the ER/early Golgi compartments. If NPxY2 had a substantial role in this, inactivation can apparently be compensated for by the membrane proximal NPxY1 motif.

Therefore we speculate that the NPxY1 motif of LRP1 is very important in early sorting steps in ER/early Golgi compartments. However, the only two interacting proteins shown so far to bind to the NPxY1 motif, FE65 and SXN17, seem to be involved in processes like amyloid precursor protein (APP) processing by bridging the LRP1 C-terminus and APP C-terminus at the cell surface and in recycling of LRP1 respectively (Pietrzik et al., 2004; van Kerkhof et al., 2005). Thus, proteins relevant for interaction with the NPxY1 domain and regulating early sorting steps are still illusive. As reviewed by Rodriguez-Boulan and Musch, sorting in the biosynthetic pathway does not only occur in the Golgi complex or the trans-Golgi network, but may even occur distally to the Golgi in recycling endosomes or, proximally to the Golgi complex at the ER exit site (Rodriguez-Boulan and Musch, 2005). Involvement of the NPxY1 motif in early sorting steps of LRP1 is an unexpected finding, but it points towards an involvement of NPxY motifs in sorting at the exit of the ER or the early Golgi. In line with our finding, Nahari and colleagues showed that a transplanted NPxY sequence in the cytosolic domain of the erythropoietin receptor enhanced maturation and cell surface expression of this receptor, which normally shows only slow exit out of the ER (Nahari et al., 2008).

Inactivation of the NPxY1 domain in LRP1 does not result in strong accumulation of LRP1-fl in the ER/early Golgi compartment, but results in proteasomal degradation. These findings suggest that inactivation of the NPXY1 domain in LRP1 triggers proteasomal degradation. Melman and colleagues showed for LRP1 mini-receptors that the proteasomal system is relevant for delivery of mature LRP1 into the degradation pathway, whereas immature LRP1 levels are hardly affected by proteasome inhibitors (Melman et al., 2002). A region of 19 amino acids, starting with the distal NPxY2 motif, seems to be required for this proteasomal regulation. It can be speculated that inactivation of the NPxY1 motif precludes interaction with the normally involved sorting mechanisms and enables premature LRP1 degradation. Future studies will investigate the mechanism of proteasomal degradation with regard to ubiquitination of LRP1. In addition to NPxY1 knock-in mutations, single amino acid substitutions within the NPxY1 motif of LRP1 mini-receptors will be generated to elucidate the critical amino acid involved in premature degradation of LRP1. In conclusion, the results presented in this study highlight a novel important role of the NPxY1 domain in early steps of LRP1 biosynthesis. This novel role might even be relevant for other lipoprotein receptors and unrelated receptors sharing NPxY motifs.

4.2. LRP1 mediates bidirectional transcytosis of amyloid-β (Aβ) across the blood-brain barrier (BBB)

The above described findings suggested to use the viable endocytosis deficient NPxY2 knock-in mouse in an Alzheimer's disease (AD) related paradigm. LRP1 has recently been suggested to mediate Aβ clearance across the BBB by a transcytotic mechanism (Shibata et al., 2000), but genetic evidence is missing due to the early embryonic lethal phenotype of LRP1 KO mice (Herz et al., 1992). Therefore, we established an *in vitro* BBB transport model to investigate LRP1-mediated Aβ transport across the BBB in more detail.

In contrast to immortalised endothelial cell (EC) lines, it has been recently shown that primary ECs derived from brain capillaries in mono-culture more closely mimic the *in vivo* BBB phenotype (Weidenfeller et al., 2005). As part of the neurovascular unit, astrocytes and/or pericytes in co-culture with rat brain ECs have been shown to increase expression levels of tight junction (TJ) proteins and transendothelial electrical resistance (TEER) values *in vitro*, hence, improving barrier properties (Daneman et al.; Nakagawa et al., 2009). Whether this mechanism results from direct interaction between the cell types or secreted factors remains to be elucidated. In addition, it has been shown that EC lines loose their BBB specific phenotype in culture (Barar et al.). Our primary mouse brain capillary EC (pMBCEC) *in vitro* BBB model confirms the expression of TJ proteins and the EC typical spindle-shaped morphology. Moreover, we were able to increase barrier tightness by serum withdrawal and addition of physiologic hydrocortisone (HC) concentrations for 24 hours as determined by TEER measurements (Figure 10).

Expression of functional LRP1 in ECs is a prerequisite to study LRP1-mediated transcytosis of Aβ across the BBB. Recent studies have already shown the expression of LRP1 in vessels within brain sections taken from human frontal cortex and (Shibata et al., 2000), additionally, in immortalised EC lines and human brain ECs by Western blotting (Deane et al., 2004; Nazer et al., 2008; Yamada et al., 2008). We were able to detect LRP1 expression in isolated pMBCECs used in our transport studies (Figure 11a). Furthermore, since LRP1 has initially been described as $\alpha_2 M$ receptor (Kristensen et al., 1990), we performed a sensitive $[^{125}I]$-$\alpha_2 M$ uptake assay to confirm the expression of functionally active LRP1 on cultured pMBCECs after serum withdrawal and HC addition (Figure 11b). These results indicate that the *in vitro* tissue culture system we are using is sufficient to analyse LRP1 mediated transport. Instead of using co-cultures of pMBCECs with astrocytes and/or pericytes, we chose to use a pMBCEC mono-culture set up due to the extremely challenging task of how to distinguish the participation of each cell type in LRP1-dependent uptake/transport mechanisms.

Several studies have identified LRP1 as a transporter for Aβ in the brain-to-blood direction across the BBB by stereotactical brain microinjection experiments with iodinated Aβ (Bell et al., 2007; Deane et al., 2008; Deane et al., 2005; Deane et al., 2004; Ito et al., 2007; Shibata et al., 2000). Deane and colleagues measured the efflux of brain-derived Aβ in heterozygous Tg2576 (APPsw$^{+/-}$) transgenic mice via LRP1 and, furthermore, LRP1-mediated uptake of Aβ by isolated brain capillaries has been determined (Deane et al., 2005; Deane et al., 2004). Although other studies have successfully applied receptor-associated protein (RAP) to block LRP1-mediated transcytosis of Aβ across the BBB (Bell et al., 2007; Deane et al., 2005; Deane et al., 2004; Shibata et al., 2000), it has been recently suggested that RAP interacts with Aβ peptides and promotes their cellular uptake by brain vascular smooth muscle cells, neuroblastoma cells, glioblastoma cells and Chinese hamster ovary cells (Kanekiyo and Bu, 2009). The promoting effect of RAP on Aβ uptake shown by Kanekiyo and colleagues might be due to the high concentrations of Aβ used that ranged from 100 nM to 1 µM. In contrast, in transcytosis and endocytosis studies using RAP and high picomolar to low nanomolar Aβ concentrations a reduction in Aβ transcytosis and Aβ uptake was detected (Bell et al., 2007; Deane et al., 2005; Deane et al., 2004; Ito et al., 2007; Nazer et al., 2008; Shibata et al., 2000; Yamada et al., 2008). In order to inhibit Aβ transcytosis many different approaches have been taken: LRP1-mediated transcytosis has been inhibited with RAP, antibodies against α$_2$M or LRP1 (Bell et al., 2007; Deane et al., 2008; Deane et al., 2004; Shibata et al., 2000), as well as LRP1 ligands α$_2$M, apolipoprotein isoforms E2-4 and lactoferrin (Ito et al., 2006). Since we used radiolabelled Aβ$_{1-40}$ in our *in vitro* assays we had to proof the integrity of the radiolabelled protein. Therefore, we measured the disintegration of [^{125}I]-Aβ$_{1-40}$ over various time points. Due to the minor spontaneous disintegration of [^{125}I] from [^{125}I]-Aβ$_{1-40}$ during 6 hours we only considered trichloroacetic acid precipitable intact [^{125}I]-Aβ$_{1-40}$ in our transcytosis studies (Figure 12). When using radiolabelled Aβ, an additional approach towards decreased clearance of radiolabelled Aβ from the brain can be performed by

coadministration of excess amounts of unlabelled Aβ. However, it has been shown that Aβ dimers are cleared at a much slower rate than the monomers and that high levels of Aβ can favour the aggregation into multimers, therefore, complicating interpretation of the results (Ito et al., 2007). To determine the aggregation state of the Aβ peptides in our experiments, we performed SDS-PAGE and subsequent autoradiography and we were able to exclude [^{125}I]-Aβ$_{1-40}$ aggregates under these conditions (Figure 12c).

For our studies, we chose to investigate LRP1-mediated transcytosis of [^{125}I]-Aβ$_{1-40}$ at pathophysiological concentrations across an *in vitro* BBB model consisting of primary ECs. Since Aβ$_{1-40}$ is cleared much faster than Aβ$_{1-42}$ we investigated LRP1-mediated transcytosis of the shorter isoform. Furthermore, it has been suggested that Aβ$_{1-40}$ is cleared at the BBB by a transport-dependent mechanism whereas Aβ$_{1-42}$ clearance is more catabolism-dependent (Zlokovic et al., 2000). As demonstrated by several groups, inhibition of Aβ transport by LRP1 was achieved using RAP and the data presented in this study are in agreement with previous studies showing a RAP mediated strong inhibition of Aβ transport (Bell et al., 2007; Deane et al., 2005; Deane et al., 2004; Shibata et al., 2000). RAP blocked Aβ transport from the brain compartment into the blood compartment at each time point of the 6 hour time course experiment (Figure 13a). Furthermore, we were able to show that RAP decreases the amount of [^{125}I]-Aβ$_{1-40}$ transcytosed to the luminal membrane compared to control condition providing first evidence for LRP1 mediated transcytosis (Figure 13c). Surprisingly, RAP did not prevent binding of Aβ to the abluminal membrane. This might be due to the fact that Aβ can form a complex with RAP as described by Kanekiyo and colleagues, or because Aβ also binds to other components of the cell membrane (Verdier et al., 2004).

Recently, an *in vitro* BBB model using Madin Darby Canine Kidney (MDCK) cells stably transfected with an LRP1 mini-receptor consisting of the complete β-subunit and ligand binding domain IV failed to show the existence of [^{125}I]-Aβ$_{1-40}$ transcytosis across the tight monolayer (Nazer et al., 2008). Instead, the authors showed that MDCKs expressing the

LRP1 mini-receptor endocytose and degrade Aβ. MDCK cells are of epithelial origins, hence, LRP1 might have a different function in this cell type compared to endothelial LRP1. This assumption is underlined by studies showing uptake and degradation of circulating Aβ in the kidney which is mainly composed of cells of epithelial characters (Sagare et al., 2007). Additionally, overexpression of the truncated LRP1 mini-receptor on top of endogenous LRP1 in MDCK cells might lead to an increased lysosomal degradation of the mini-receptors and, therefore, an increased degradation of potentially transported Aβ. In all experiments performed with our endothelial BBB model expressing endogenous LRP1, we did not observe a role for LRP1 in $[^{125}I]$-A$β_{1-40}$ degradation during transcytosis when we analysed the ratio of intact versus degraded Aβ in the acceptor compartment (Figures 13-15). Considering the actual ratio ranging from 0.4 to 0.8 in the acceptor compartment at the end of the study suggests that at least 30% of all $[^{125}I]$ counts detected were derived from intact $[^{125}I]$-A$β_{1-40}$. This is in contrast to the transport study performed with MDCKs stably expressing LRP1 mini-receptor where virtually all of the $[^{125}I]$ counts in the acceptor compartment were from degraded $[^{125}I]$-A$β_{1-40}$ (Nazer et al., 2008). The observed decrease in the ratio of inputs compared to acceptor compartments in our studies can be explained by free $[^{125}I]$ diffusing through the pMBCEC monolayer. Whereas $[^{125}I]$-A$β_{1-40}$ is transcytosed to a limited degree free $[^{125}I]$ can easily pass the monolayer. This inverts the ratio towards more free $[^{125}I]$ in the acceptor compartment which is not due to LRP1-mediated degradation of $[^{125}I]$-A$β_{1-40}$.

In our 6 hour time course transport study from brain-to-blood compartment we observed a plateau phase between 2 and 6 hours for LRP1-mediated transport of intact $[^{125}I]$-A$β_{1-40}$ across the pMBCEC monolayer (Figure 13a). Therefore, we investigated if LRP1 can also transcytose Aβ in the blood-to-brain direction and found a significant LRP1-mediated transport of Aβ (Figures 14a and 15d). To date, this transport has not been observed for LRP1 but was rather contributed to a different receptor. Receptor-mediated transcytosis of Aβ from the blood into the brain has been described for the receptor for advanced glycation

endproducts (RAGE) (Deane et al., 2003). Since we could not detect RAGE mRNA (data not shown) or protein (Figure 11a) in our pMBCEC analyses, we did not perform RAGE-mediated Aβ transport studies. The physiological relevance of LRP1-mediated Aβ transcytosis from blood-to-brain remains to be elucidated in further experimental set ups. Under *in vivo* conditions, the LRP1-Aβ complex that transcytoses to the luminal membrane can subsequently be cleaved, resulting in the liberation of a complex consisting of soluble LRP1 and Aβ that is targeted for degradation by the liver, kidney and spleen (Sagare et al., 2007).

Although some studies have identified an impaired Aβ clearance phenotype due to LRP1 downregulation in both *in vivo* and *in vitro* studies (Bell et al., 2009; Deane et al., 2004; Jaeger et al., 2009; Yamada et al., 2008), genetic evidence for LRP1-mediated transport of Aβ across the BBB was lacking due to the embryonic lethal phenotype of LRP1 KO mice (Herz et al., 1992). We, for the first time, provide genetic evidence for LRP1-mediated transcytosis of Aβ across pMBCEC monolayers generated from LRP1 knock-in mice containing a mutation in the NPxY2 endocytosis/sorting motif (Roebroek et al., 2006). In comparison to pMBCECs derived from WT littermate controls, NPxY2 mutant pMBCEC monolayers transcytosed significantly less $[^{125}I]$-Aβ$_{1-40}$ in the brain-to-blood and blood-to-brain direction (Figure 15a and c). The underlying mechanism for decreased Aβ transcytosis can be explained as follows: (1) mutation of the endocytosis motif results in diminished internalisation of the receptor-ligand complex, which we have shown using α$_2$M (Figure 9) (Reekmans et al., 2009), and/or (2) disruption of the sorting motif impairs predominant targeting of LRP1 to the abluminal membrane, eventually resulting in decreased LRP1 levels at this membrane compared to WT monolayers (Marzolo et al., 2003).
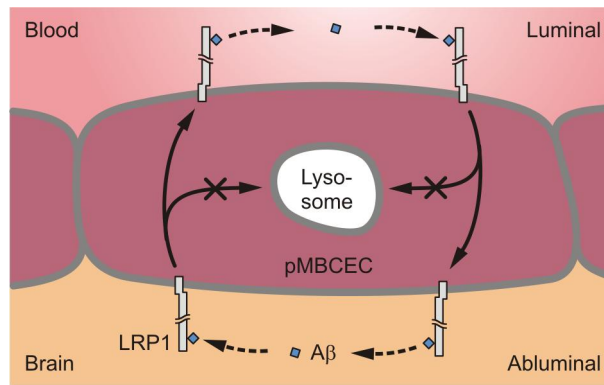
Figure 16 Low density lipoprotein receptor-related protein 1 (LRP1) expressed in primary mouse brain capillary endothelial cells (pMBCECs) is a receptor for bidirectional transcytosis of amyloid-β 1-40 (Aβ$_{1-40}$) across the *in vitro* blood-brain barrier and does not participate in Aβ$_{1-40}$ degradation during transcytosis.

Finally, we conclude that LRP1 is a bona-fide receptor involved in bidirectional transcytosis of Aβ across the BBB as demonstrated by the decreased clearance across pMBCEC monolayers (Figure 16). This was achieved by ligand binding inhibition experiments and genetic modification of the endogenous LRP1 gene through a knock-in mutation of the NPxY2 motif, resulting in reduced Aβ transcytosis. Therefore, LRP1 might be considered as a potential modulater of toxic, soluble Aβ in the brain parenchyma. Based on our *in vitro* results we conclude that LRP1 mediates Aβ transcytosis across the BBB in both directions at similar rates. Future studies will investigate the role of LRP1 in blood-to-brain transport of Aβ under *in vivo* conditions to verify the physiologic relevance of this mechanism. One possibility to investigate the relevance of luminally expressed LRP1 is to study the transport of apoliporotein E (apoE), a ligand of LRP1, into the brain. Previously, transport of pre-complexed apoE-Aβ$_{1-40}$ from the blood into the brain has been demonstrated (Martel et al., 1997). In addition, it has been shown that expression of apoE reduces Aβ deposition in a mouse model of AD and, therefore, LRP1 could transcytose circulating apoE into the brain (Holtzman et al., 1999). This will aid greater understanding of AD pathogenesis at the BBB.

4.3. Summary

Studies on the physiological role of endogenous LRP1 have been hindered by the early embryonic lethal phenotype of LRP1 KO mice (Herz et al., 1992). To overcome this problem, LRP1 knock-in mice were generated by RMCE. The endogenous LRP1 gene was modified at gene regions encoding the two cytoplasmic NPxY motifs involved in receptor endocytosis and recycling. Alanine subsititutions within the NPxY domains (NPxY $\rightarrow$ AAxA) caused distinct phenotypes in LRP1 knock-in mice. Whereas the NPxY2 mouse was viable and fertile, NPxY1 and NPxY1+2 mice showed an embryonic to perinatal lethal phenotype mimicking the complete LRP1 KO (Reekmans et al., 2009; Roebroek et al., 2006). Here we show that the lethal phenotype of NPxY1 and NPxY1+2 knock-in mice is due to premature proteasomal degradation of immature LRP1, thereby, preventing the generation of mature LRP1. In addition, mutation of the dominant motif for LRP1-mediated ligand endocytosis resulted in a decreased capability of LRP1 to internalise α_2M. The reduced endocytosis in NPxY2 MEFs and the viable phenotype of NPxY2 mice were used to investigate a disease related paradigm in more detail. AD is characterised by increased brain levels of neurotoxic Aβ. Ligand binding inhibition experiments revealed that LRP1 mediates Aβ clearance across the BBB from brain-to-blood, therefore, representing a target for therapeutic intervention. However, this mechanism is controversial due to the lack of genetic proof. For the first time, we provide genetic evidence for LRP1-mediated bidirectional Aβ transcytosis across the BBB by using endocytosis deficient pMBCECs generated from NPxY2 knock-in mice.

5. ABSTRACT

Analyses of low density lipoprotein receptor-related protein 1 (LRP1) mutant mouse embryonic fibroblasts (MEFs) generated from LRP1 knock-in mice revealed that inefficient maturation and premature proteasomal degradation of immature LRP1 is causing early embryonic lethality in NPxY1 and NPxY1+2 mutant mice. Single inactivation of the distal NPxY2 motif showed no obvious phenotypic differences compared to wild-type (WT). In MEFs, NPxY2 mutant LRP1 showed efficient maturation but, as expected, decreased endocytosis. The single proximal NPxY1 and the double mutant NPxY1+2 were unable to reach the cell surface as an endocytic receptor due to premature degradation. In conclusion, the proximal NPxY1 and distal NPxY2 motifs are not only relevant for basolateral sorting, endocytosis and signalling, but they are, especially the proximal NPxY1 motif, also essential for early sorting steps in the biosynthesis of mature LRP1.

According to the 'amyloid hypothesis', the amyloid-β (Aβ) peptide is the toxic intermediate driving Alzheimer's Disease pathogenesis. Recent evidence suggests that LRP1 transcytoses Aβ out of the brain across the blood-brain barrier (BBB). To provide genetic evidence for LRP1-mediated transcytosis of Aβ across the BBB we analysed Aβ transcytosis across primary mouse brain capillary endothelial cells (pMBCECs) derived from WT and LRP1 knock-in mice. Here, we show that pMBCECs *in vitro* express functionally active LRP1. Moreover, we demonstrate that LRP1 mediates transcytosis of $[^{125}I]$-Aβ$_{1-40}$ across pMBCECs in both directions, whereas no role for LRP1-mediated Aβ degradation was detected. Analysis of $[^{125}I]$-Aβ$_{1-40}$ transport across pMBCECs generated from mice harbouring a knock-in mutation in the NPxY2 endocytosis/sorting domain of endogenous LRP1 revealed a reduced Aβ clearance from brain-to-blood and blood-to-brain compared to WT derived pMBCECs. Therefore, for the first time, we present genetic evidence that LRP1 modulates the pathogenic actions of soluble Aβ in the brain by clearing Aβ across the BBB.

6. REFERENCES

Abbott, N.J., Ronnback L., Hansson E., 2006. Astrocyte-endothelial interactions at the blood-brain barrier. Nat Rev Neurosci 7, 41-53.

Akanuma, S., Ohtsuki S., Doi Y., Tachikawa M., Ito S., Hori S., Asashima T., Hashimoto T., Yamada K., Ueda K., Iwatsubo T., Terasaki T., 2008. ATP-binding cassette transporter A1 (ABCA1) deficiency does not attenuate the brain-to-blood efflux transport of human amyloid-beta peptide (1-40) at the blood-brain barrier. Neurochem Int 52, 956-961.

Barar, J., Gumbleton M., Asadi M., Omidi Y., Barrier functionality and transport machineries of human ECV304 cells. Med Sci Monit 16, BR52-60.

Bell, R.D., Deane R., Chow N., Long X., Sagare A., Singh I., Streb J.W., Guo H., Rubio A., Van Nostrand W., Miano J.M., Zlokovic B.V., 2009. SRF and myocardin regulate LRP-mediated amyloid-beta clearance in brain vascular cells. Nat Cell Biol 11, 143-153.

Bell, R.D., Sagare A.P., Friedman A.E., Bedi G.S., Holtzman D.M., Deane R., Zlokovic B.V., 2007. Transport pathways for clearance of human Alzheimer's amyloid beta-peptide and apolipoproteins E and J in the mouse central nervous system. J Cereb Blood Flow Metab 27, 909-918.

Blanc, E.M., Toborek M., Mark R.J., Hennig B., Mattson M.P., 1997. Amyloid beta-peptide induces cell monolayer albumin permeability, impairs glucose transport, and induces apoptosis in vascular endothelial cells. J Neurochem 68, 1870-1881.

Bouras, C., Kovari E., Herrmann F.R., Rivara C.B., Bailey T.L., von Gunten A., Hof P.R., Giannakopoulos P., 2006. Stereologic analysis of microvascular morphology in the elderly: Alzheimer disease pathology and cognitive status. J Neuropathol Exp Neurol 65, 235-244.

Bowman, G.L., Kaye J.A., Moore M., Waichunas D., Carlson N.E., Quinn J.F., 2007. Blood-brain barrier impairment in Alzheimer disease: stability and functional significance. Neurology 68, 1809-1814.

Carmeliet, P., Jain R.K., 2000. Angiogenesis in cancer and other diseases. Nature 407, 249-257.

Cirrito, J.R., Deane R., Fagan A.M., Spinner M.L., Parsadanian M., Finn M.B., Jiang H., Prior J.L., Sagare A., Bales K.R., Paul S.M., Zlokovic B.V., Piwnica-Worms D., Holtzman D.M., 2005. P-glycoprotein deficiency at the blood-brain barrier increases amyloid-beta deposition in an Alzheimer disease mouse model. J Clin Invest 115, 3285-3290.

Daneman, R., Zhou L., Kebede A.A., Barres B.A., Pericytes are required for blood-brain barrier integrity during embryogenesis. Nature,

Dean, M., Hamon Y., Chimini G., 2001. The human ATP-binding cassette (ABC) transporter superfamily. J Lipid Res 42, 1007-1017.

Deane, R., Du Yan S., Submamaryan R.K., LaRue B., Jovanovic S., Hogg E., Welch D., Manness L., Lin C., Yu J., Zhu H., Ghiso J., Frangione B., Stern A., Schmidt A.M., Armstrong D.L., Arnold B., Liliensiek B., Nawroth P., Hofman F., Kindy M., Stern D., Zlokovic B., 2003. RAGE mediates amyloid-beta peptide transport across the blood-brain barrier and accumulation in brain. Nat Med 9, 907-913.

Deane, R., Sagare A., Hamm K., Parisi M., Lane S., Finn M.B., Holtzman D.M., Zlokovic B.V., 2008. apoE isoform-specific disruption of amyloid beta peptide clearance from mouse brain. J Clin Invest 118, 4002-4013.

Deane, R., Sagare A., Hamm K., Parisi M., LaRue B., Guo H., Wu Z., Holtzman D.M., Zlokovic B.V., 2005. IgG-assisted age-dependent clearance of Alzheimer's amyloid beta peptide by the blood-brain barrier neonatal Fc receptor. J Neurosci 25, 11495-11503.

Deane, R., Wu Z., Sagare A., Davis J., Du Yan S., Hamm K., Xu F., Parisi M., LaRue B., Hu H.W., Spijkers P., Guo H., Song X., Lenting P.J., Van Nostrand W.E., Zlokovic B.V., 2004. LRP/amyloid beta-peptide interaction mediates differential brain efflux of Abeta isoforms. Neuron 43, 333-344.

Desai, B.S., Schneider J.A., Li J.L., Carvey P.M., Hendey B., 2009. Evidence of angiogenic vessels in Alzheimer's disease. J Neural Transm 116, 587-597.

Dickson, R.B., Willingham M.C., Pastan I., 1981. Binding and internalization of 125I-alpha 2-macroglobulin by cultured fibroblasts. J Biol Chem 256, 3454-3459.

Dieckmann, M., Dietrich M.F., Herz J., Lipoprotein receptors - an evolutionarily ancient multifunctional receptor family. Biol Chem 391, 1341-1363.

Doyle, L.A., Yang W., Abruzzo L.V., Krogmann T., Gao Y., Rishi A.K., Ross D.D., 1998. A multidrug resistance transporter from human MCF-7 breast cancer cells. Proc Natl Acad Sci U S A 95, 15665-15670.

Farris, W., Schutz S.G., Cirrito J.R., Shankar G.M., Sun X., George A., Leissring M.A., Walsh D.M., Qiu W.Q., Holtzman D.M., Selkoe D.J., 2007. Loss of neprilysin function promotes amyloid plaque formation and causes cerebral amyloid angiopathy. Am J Pathol 171, 241-251.

Folin, M., Baiguera S., Tommasini M., Guidolin D., Conconi M.T., De Carlo E., Nussdorfer G.G., Parnigotto P.P., 2005. Effects of beta-amyloid on rat neuromicrovascular endothelial cells cultured in vitro. Int J Mol Med 15, 929-935.

Gonzalez-Velasquez, F.J., Kotarek J.A., Moss M.A., 2008. Soluble aggregates of the amyloid-beta protein selectively stimulate permeability in human brain microvascular endothelial monolayers. J Neurochem 107, 466-477.

Grieb, P., Forster R.E., Strome D., Goodwin C.W., Pape P.C., 1985. O2 exchange between blood and brain tissues studied with 18O2 indicator-dilution technique. J Appl Physiol 58, 1929-1941.

Herz, J., Clouthier D.E., Hammer R.E., 1992. LDL receptor-related protein internalizes and degrades uPA-PAI-1 complexes and is essential for embryo implantation. Cell 71, 411-421.

Herz, J., Strickland D.K., 2001. LRP: a multifunctional scavenger and signaling receptor. J Clin Invest 108, 779-784.

Higgins, C.F., 1992. ABC transporters: from microorganisms to man. Annu Rev Cell Biol 8, 67-113.

Hildenbrand, R., Allgayer H., Marx A., Stroebel P., Modulators of the urokinase-type plasminogen activation system for cancer. Expert Opin Investig Drugs 19, 641-652.

Holtzman, D.M., Bales K.R., Wu S., Bhat P., Parsadanian M., Fagan A.M., Chang L.K., Sun Y., Paul S.M., 1999. Expression of human apolipoprotein E reduces amyloid-beta deposition in a mouse model of Alzheimer's disease. J Clin Invest 103, R15-R21.

Ito, S., Ohtsuki S., Kamiie J., Nezu Y., Terasaki T., 2007. Cerebral clearance of human amyloid-beta peptide (1-40) across the blood-brain barrier is reduced by self-aggregation and formation of low-density lipoprotein receptor-related protein-1 ligand complexes. J Neurochem 103, 2482-2490.

Ito, S., Ohtsuki S., Terasaki T., 2006. Functional characterization of the brain-to-blood efflux clearance of human amyloid-beta peptide (1-40) across the rat blood-brain barrier. Neurosci Res 56, 246-252.

Iwata, N., Tsubuki S., Takaki Y., Shirotani K., Lu B., Gerard N.P., Gerard C., Hama E., Lee H.J., Saido T.C., 2001. Metabolic regulation of brain Abeta by neprilysin. Science 292, 1550-1552.

Jaeger, L.B., Dohgu S., Sultana R., Lynch J.L., Owen J.B., Erickson M.A., Shah G.N., Price T.O., Fleegal-Demotta M.A., Butterfiled D.A., Banks W.A., 2009. Lipopolysaccharide alters the blood-brain barrier transport of amyloid beta protein: a mechanism for

inflammation in the progression of Alzheimer's disease. Brain Behav Immun 23, 507-517.

Kanekiyo, T., Bu G., 2009. Receptor-associated protein interacts with amyloid-beta peptide and promotes its cellular uptake. J Biol Chem 284, 33352-33359.

Kang, D.E., Pietrzik C.U., Baum L., Chevallier N., Merriam D.E., Kounnas M.Z., Wagner S.L., Troncoso J.C., Kawas C.H., Katzman R., Koo E.H., 2000. Modulation of amyloid beta-protein clearance and Alzheimer's disease susceptibility by the LDL receptor-related protein pathway. J Clin Invest 106, 1159-1166.

Kristensen, T., Moestrup S.K., Gliemann J., Bendtsen L., Sand O., Sottrup-Jensen L., 1990. Evidence that the newly cloned low-density-lipoprotein receptor related protein (LRP) is the alpha 2-macroglobulin receptor. FEBS Lett 276, 151-155.

Kuhnke, D., Jedlitschky G., Grube M., Krohn M., Jucker M., Mosyagin I., Cascorbi I., Walker L.C., Kroemer H.K., Warzok R.W., Vogelgesang S., 2007. MDR1-P-Glycoprotein (ABCB1) Mediates Transport of Alzheimer's amyloid-beta peptides--implications for the mechanisms of Abeta clearance at the blood-brain barrier. Brain Pathol 17, 347-353.

LaRue, B., Hogg E., Sagare A., Jovanovic S., Maness L., Maurer C., Deane R., Zlokovic B.V., 2004. Method for measurement of the blood-brain barrier permeability in the perfused mouse brain: application to amyloid-beta peptide in wild type and Alzheimer's Tg2576 mice. J Neurosci Methods 138, 233-242.

Leissring, M.A., Farris W., Chang A.Y., Walsh D.M., Wu X., Sun X., Frosch M.P., Selkoe D.J., 2003. Enhanced proteolysis of beta-amyloid in APP transgenic mice prevents plaque formation, secondary pathology, and premature death. Neuron 40, 1087-1093.

Li, Y., Marzolo M.P., van Kerkhof P., Strous G.J., Bu G., 2000. The YXXL motif, but not the two NPXY motifs, serves as the dominant endocytosis signal for low density lipoprotein receptor-related protein. J Biol Chem 275, 17187-17194.

Mackic, J.B., Stins M., McComb J.G., Calero M., Ghiso J., Kim K.S., Yan S.D., Stern D., Schmidt A.M., Frangione B., Zlokovic B.V., 1998. Human blood-brain barrier receptors for Alzheimer's amyloid-beta 1- 40. Asymmetrical binding, endocytosis, and transcytosis at the apical side of brain microvascular endothelial cell monolayer. J Clin Invest 102, 734-743.

Madara, J.L., 1988. Tight junction dynamics: is paracellular transport regulated? Cell 53, 497-498.

Martel, C.L., Mackic J.B., Matsubara E., Governale S., Miguel C., Miao W., McComb J.G., Frangione B., Ghiso J., Zlokovic B.V., 1997. Isoform-specific effects of apolipoproteins E2, E3, and E4 on cerebral capillary sequestration and blood-brain barrier transport of circulating Alzheimer's amyloid beta. J Neurochem 69, 1995-2004.

Martin, A.M., Kuhlmann C., Trossbach S., Jaeger S., Waldron E., Roebroek A., Luhmann H.J., Laatsch A., Weggen S., Lessmann V., Pietrzik C.U., 2008. The functional role of the second NPXY motif of the LRP1 beta-chain in tissue-type plasminogen activator-mediated activation of N-methyl-D-aspartate receptors. J Biol Chem 283, 12004-12013.

Marzolo, M.P., Yuseff M.I., Retamal C., Donoso M., Ezquer F., Farfan P., Li Y., Bu G., 2003. Differential distribution of low-density lipoprotein-receptor-related protein (LRP) and megalin in polarized epithelial cells is determined by their cytoplasmic domains. Traffic 4, 273-288.

Melman, L., Geuze H.J., Li Y., McCormick L.M., Van Kerkhof P., Strous G.J., Schwartz A.L., Bu G., 2002. Proteasome regulates the delivery of LDL receptor-related protein into the degradation pathway. Mol Biol Cell 13, 3325-3335.

Moestrup, S.K., Gliemann J., Pallesen G., 1992. Distribution of the alpha 2-macroglobulin receptor/low density lipoprotein receptor-related protein in human tissues. Cell Tissue Res 269, 375-382.

Nahari, T., Barzilay E., Hirschberg K., Neumann D., 2008. A transplanted NPVY sequence in the cytosolic domain of the erythropoietin receptor enhances maturation. Biochem J 410, 409-416.

Nakagawa, S., Deli M.A., Kawaguchi H., Shimizudani T., Shimono T., Kittel A., Tanaka K., Niwa M., 2009. A new blood-brain barrier model using primary rat brain endothelial cells, pericytes and astrocytes. Neurochem Int 54, 253-263.

Nazer, B., Hong S., Selkoe D.J., 2008. LRP promotes endocytosis and degradation, but not transcytosis, of the amyloid-beta peptide in a blood-brain barrier in vitro model. Neurobiol Dis 30, 94-102.

Neels, J.G., van Den Berg B.M., Lookene A., Olivecrona G., Pannekoek H., van Zonneveld A.J., 1999. The second and fourth cluster of class A cysteine-rich repeats of the low density lipoprotein receptor-related protein share ligand-binding properties. J Biol Chem 274, 31305-31311.

Orth, K., Madison E.L., Gething M.J., Sambrook J.F., Herz J., 1992. Complexes of tissue-type plasminogen activator and its serpin inhibitor plasminogen-activator inhibitor type 1 are internalized by means of the low density lipoprotein receptor-related protein/alpha 2-macroglobulin receptor. Proc Natl Acad Sci U S A 89, 7422-7426.

Pahnke, J., Walker L.C., Scheffler K., Krohn M., 2009. Alzheimer's disease and blood-brain barrier function-Why have anti-beta-amyloid therapies failed to prevent dementia progression? Neurosci Biobehav Rev,

Pardridge, W.M., Eisenberg J., Yang J., 1985. Human blood-brain barrier insulin receptor. J Neurochem 44, 1771-1778.

Perriere, N., Demeuse P., Garcia E., Regina A., Debray M., Andreux J.P., Couvreur P., Scherrmann J.M., Temsamani J., Couraud P.O., Deli M.A., Roux F., 2005. Puromycin-based purification of rat brain capillary endothelial cell cultures. Effect on the expression of blood-brain barrier-specific properties. J Neurochem 93, 279-289.

Pflanzner, T., Kuhlmann C.R.W., Pietrzik C.U., in press. Blood-brain barrier models for the investigation of transporter- and receptor-mediated amyloid-β clearance in Alzheimer's disease. Curr Alzheimer Res,

Pietrzik, C.U., Busse T., Merriam D.E., Weggen S., Koo E.H., 2002. The cytoplasmic domain of the LDL receptor-related protein regulates multiple steps in APP processing. Embo J 21, 5691-5700.

Pietrzik, C.U., Yoon I.S., Jaeger S., Busse T., Weggen S., Koo E.H., 2004. FE65 constitutes the functional link between the low-density lipoprotein receptor-related protein and the amyloid precursor protein. J Neurosci 24, 4259-4265.

Preston, S.D., Steart P.V., Wilkinson A., Nicoll J.A., Weller R.O., 2003. Capillary and arterial cerebral amyloid angiopathy in Alzheimer's disease: defining the perivascular route for the elimination of amyloid beta from the human brain. Neuropathol Appl Neurobiol 29, 106-117.

Reekmans, S.M., Pflanzner T., Gordts P.L., Isbert S., Zimmermann P., Annaert W., Weggen S., Roebroek A.J., Pietrzik C.U., 2009. Inactivation of the proximal NPXY motif impairs early steps in LRP1 biosynthesis. Cell Mol Life Sci,

Reekmans, S.M., Pflanzner T., Gordts P.L., Isbert S., Zimmermann P., Annaert W., Weggen S., Roebroek A.J., Pietrzik C.U., 2010. Inactivation of the proximal NPXY motif impairs early steps in LRP1 biosynthesis. Cell Mol Life Sci 67, 135-145.

Rodriguez-Boulan, E., Musch A., 2005. Protein sorting in the Golgi complex: shifting paradigms. Biochim Biophys Acta 1744, 455-464.

Roebroek, A.J., Reekmans S., Lauwers A., Feyaerts N., Smeijers L., Hartmann D., 2006. Mutant Lrp1 knock-in mice generated by recombinase-mediated cassette exchange reveal differential importance of the NPXY motifs in the intracellular domain of LRP1 for normal fetal development. Mol Cell Biol 26, 605-616.

Sagare, A., Deane R., Bell R.D., Johnson B., Hamm K., Pendu R., Marky A., Lenting P.J., Wu Z., Zarcone T., Goate A., Mayo K., Perlmutter D., Coma M., Zhong Z., Zlokovic B.V., 2007. Clearance of amyloid-beta by circulating lipoprotein receptors. Nat Med 13, 1029-1031.

Sappino, A.P., Huarte J., Belin D., Vassalli J.D., 1989. Plasminogen activators in tissue remodeling and invasion: mRNA localization in mouse ovaries and implanting embryos. J Cell Biol 109, 2471-2479.

Schlachetzki, F., Zhu C., Pardridge W.M., 2002. Expression of the neonatal Fc receptor (FcRn) at the blood-brain barrier. J Neurochem 81, 203-206.

Schmidt, A.M., Mora R., Cao R., Yan S.D., Brett J., Ramakrishnan R., Tsang T.C., Simionescu M., Stern D., 1994. The endothelial cell binding site for advanced glycation end products consists of a complex: an integral membrane protein and a lactoferrin-like polypeptide. J Biol Chem 269, 9882-9888.

Shibata, M., Yamada S., Kumar S.R., Calero M., Bading J., Frangione B., Holtzman D.M., Miller C.A., Strickland D.K., Ghiso J., Zlokovic B.V., 2000. Clearance of Alzheimer's amyloid-ss(1-40) peptide from brain by LDL receptor-related protein-1 at the blood-brain barrier. J Clin Invest 106, 1489-1499.

Simister, N.E., Mostov K.E., 1989. An Fc receptor structurally related to MHC class I antigens. Nature 337, 184-187.

Tai, L.M., Loughlin A.J., Male D.K., Romero I.A., 2009. P-glycoprotein and breast cancer resistance protein restrict apical-to-basolateral permeability of human brain endothelium to amyloid-beta. J Cereb Blood Flow Metab 29, 1079-1083.

Tanzi, R.E., Moir R.D., Wagner S.L., 2004. Clearance of Alzheimer's Abeta peptide: the many roads to perdition. Neuron 43, 605-608.

Tartakoff, A.M., 1983. Perturbation of vesicular traffic with the carboxylic ionophore monensin. Cell 32, 1026-1028.

Thomas, T., Thomas G., McLendon C., Sutton T., Mullan M., 1996. beta-Amyloid-mediated vasoactivity and vascular endothelial damage. Nature 380, 168-171.

Utter, S., Tamboli I.Y., Walter J., Upadhaya A.R., Birkenmeier G., Pietrzik C.U., Ghebremedhin E., Thal D.R., 2008. Cerebral small vessel disease-induced apolipoprotein E leakage is associated with Alzheimer disease and the accumulation of amyloid beta-protein in perivascular astrocytes. J Neuropathol Exp Neurol 67, 842-856.

Van Eck, M., Pennings M., Hoekstra M., Out R., Van Berkel T.J., 2005. Scavenger receptor BI and ATP-binding cassette transporter A1 in reverse cholesterol transport and atherosclerosis. Curr Opin Lipidol 16, 307-315.

van Kerkhof, P., Lee J., McCormick L., Tetrault E., Lu W., Schoenfish M., Oorschot V., Strous G.J., Klumperman J., Bu G., 2005. Sorting nexin 17 facilitates LRP recycling in the early endosome. Embo J 24, 2851-2861.

Verdier, Y., Zarandi M., Penke B., 2004. Amyloid beta-peptide interactions with neuronal and glial cell plasma membrane: binding sites and implications for Alzheimer's disease. J Pept Sci 10, 229-248.

von Einem, B., Schwanzar D., Rehn F., Beyer A.S., Weber P., Wagner M., Schneckenburger H., von Arnim C.A., The role of low-density receptor-related protein 1 (LRP1) as a competitive substrate of the amyloid precursor protein (APP) for BACE1. Exp Neurol 225, 85-93.

Vukic, V., Callaghan D., Walker D., Lue L.F., Liu Q.Y., Couraud P.O., Romero I.A., Weksler B., Stanimirovic D.B., Zhang W., 2009. Expression of inflammatory genes induced by beta-amyloid peptides in human brain endothelial cells and in Alzheimer's brain is mediated by the JNK-AP1 signaling pathway. Neurobiol Dis 34, 95-106.

Wahrle, S.E., Jiang H., Parsadanian M., Hartman R.E., Bales K.R., Paul S.M., Holtzman D.M., 2005. Deletion of Abca1 increases Abeta deposition in the PDAPP transgenic mouse model of Alzheimer disease. J Biol Chem 280, 43236-43242.

Wang, N., Tall A.R., 2003. Regulation and mechanisms of ATP-binding cassette transporter A1-mediated cellular cholesterol efflux. Arterioscler Thromb Vasc Biol 23, 1178-1184.

Weidenfeller, C., Schrot S., Zozulya A., Galla H.J., 2005. Murine brain capillary endothelial cells exhibit improved barrier properties under the influence of hydrocortisone. Brain Res 1053, 162-174.

Willnow, T.E., Moehring J.M., Inocencio N.M., Moehring T.J., Herz J., 1996. The low-density-lipoprotein receptor-related protein (LRP) is processed by furin in vivo and in vitro. Biochem J 313 (Pt 1), 71-76.

Wu, Z., Guo H., Chow N., Sallstrom J., Bell R.D., Deane R., Brooks A.I., Kanagala S., Rubio A., Sagare A., Liu D., Li F., Armstrong D., Gasiewicz T., Zidovetzki R., Song X., Hofman F., Zlokovic B.V., 2005. Role of the MEOX2 homeobox gene in neurovascular dysfunction in Alzheimer disease. Nat Med 11, 959-965.

Xie, J., Reverdatto S., Frolov A., Hoffmann R., Burz D.S., Shekhtman A., 2008. Structural basis for pattern recognition by the receptor for advanced glycation end products (RAGE). J Biol Chem 283, 27255-27269.

Xiong, H., Callaghan D., Jones A., Bai J., Rasquinha I., Smith C., Pei K., Walker D., Lue L.F., Stanimirovic D., Zhang W., 2009. ABCG2 is upregulated in Alzheimer's brain with cerebral amyloid angiopathy and may act as a gatekeeper at the blood-brain barrier for Abeta(1-40) peptides. J Neurosci 29, 5463-5475.

Yamada, K., Hashimoto T., Yabuki C., Nagae Y., Tachikawa M., Strickland D.K., Liu Q., Bu G., Basak J.M., Holtzman D.M., Ohtsuki S., Terasaki T., Iwatsubo T., 2008. The low

density lipoprotein receptor-related protein 1 mediates uptake of amyloid beta peptides in an in vitro model of the blood-brain barrier cells. J Biol Chem 283, 34554-34562.

Zhang, Y., Pardridge W.M., 2001. Rapid transferrin efflux from brain to blood across the blood-brain barrier. J Neurochem 76, 1597-1600.

Zlokovic, B.V., Yamada S., Holtzman D., Ghiso J., Frangione B., 2000. Clearance of amyloid beta-peptide from brain: transport or metabolism? Nat Med 6, 718.

7. PUBLICATIONS

Pflanzner T, Kuhlmann CR, Pietrzik CU. Blood-Brain-Barrier Models for the Investigation of Transporter- and Receptor-Mediated Amyloid-β Clearance in Alzheimer's Disease. *Curr Alzheimer Res*, 2010 [Epub ahead of print].

Pflanzner T, Janko MC, André-Dohmen B, Reuss S, Weggen S, Roebroek AJ, Kuhlmann CR, Pietrzik CU. LRP1 mediates bidirectional transcytosis of amyloid-β across the blood-brain barrier. *Neurobiol Aging*, 2010 [Epub ahead of print].

Reekmans SM[*], **Pflanzner T**[*], Gordts PL[*], Isbert S, Zimmermann P, Annaert W, Weggen S, Roebroek AJ[#], Pietrzik CU[#]. Inactivation of the proximal NPXY motif impairs early steps in LRP1 biosynthesis. *Cell Mol Life Sci*, 2010 Jan;67(1):135-45.

Kuhlmann CR, Librizzi L, Closhen D, **Pflanzner T**, Lessmann V, Pietrzik CU, de Curtis M, Luhmann HJ. Mechanisms of C-reactive protein-induced blood-brain barrier disruption. *Stroke*, 2009 Apr;40(4):1458-66.

[*] co-first authors

[#] co-last authors

8. ACKNOWLEDGEMENTS

9. CURRICULUM VITAE

10. EIDESSTATTLICHE ERKLÄRUNG

Hiermit versichere ich an Eides statt, dass ich die vorliegende Promotionsarbeit selbstständig verfasst und nur unter Verwendung der angegebenen Hilfsmittel angefertigt habe.

Mainz, den 08.12.2010

_____

Thorsten Pflanzner

11. ADDENDUM: PUBLISHED ARTICLE OFFPRINTS